

Winter 2012

An investigation on the resonance observed in a spirally shielded twinaxial differential pair

David Richard Levine
University of New Hampshire, Durham

Follow this and additional works at: <https://scholars.unh.edu/thesis>

Recommended Citation

Levine, David Richard, "An investigation on the resonance observed in a spirally shielded twinaxial differential pair" (2012). *Master's Theses and Capstones*. 762.
<https://scholars.unh.edu/thesis/762>

This Thesis is brought to you for free and open access by the Student Scholarship at University of New Hampshire Scholars' Repository. It has been accepted for inclusion in Master's Theses and Capstones by an authorized administrator of University of New Hampshire Scholars' Repository. For more information, please contact nicole.hentz@unh.edu.

AN INVESTIGATION ON THE RESONANCE OBSERVED IN A SPIRALLY
SHIELDED TWINAXIAL DIFFERENTIAL PAIR

BY

DAVID RICHARD LEVINE

B.S.E.E., University of New Hampshire, December 2008

THESIS

Submitted to the University of New Hampshire

In Partial Fulfillment of

The Requirements for the Degree of

Master of Science

in

Electrical Engineering

December 2012

UMI Number: 1522317

All rights reserved

INFORMATION TO ALL USERS

The quality of this reproduction is dependent upon the quality of the copy submitted.

In the unlikely event that the author did not send a complete manuscript and there are missing pages, these will be noted. Also, if material had to be removed, a note will indicate the deletion.



UMI 1522317

Published by ProQuest LLC 2013. Copyright in the Dissertation held by the Author.

Microform Edition © ProQuest LLC.

All rights reserved. This work is protected against unauthorized copying under Title 17, United States Code.



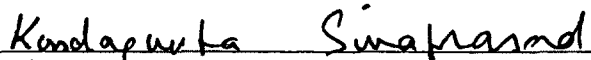
ProQuest LLC
789 East Eisenhower Parkway
P.O. Box 1346
Ann Arbor, MI 48106-1346

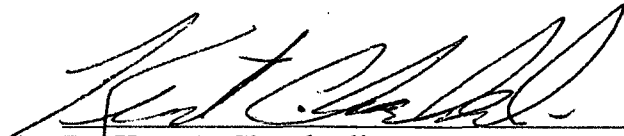
ALL RIGHTS RESERVED

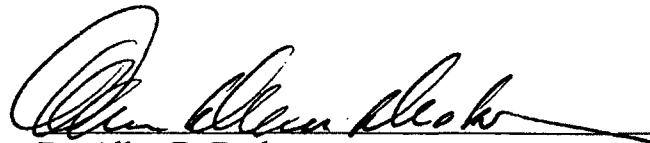
© 2012


David Richard Levine

This thesis has been examined and approved.


Thesis Director, Dr. Kondagunta U. Sivaprasad
Professor of Electrical Engineering


Dr. Kent A. Chamberlin
Professor of Electrical Engineering


Dr. Allen D. Drake
Associate Professor of Electrical Engineering


Mr. Mark W. Gailus
Principal Electrical Engineer, Amphenol TCS

12/4/12
Date

DEDICATION

To my parents

Joseph Levine and Deborah Levine

for their inspiration

To my sister

Rachael Levine

for her support

ACKNOWLEDGEMENTS

I would like to formally thank Professor Kondagunta Sivaprasad, Mr. Marc Cartier, Mr. Mark Gailus, Professor Allen Drake and Professor Kent Chamberlin for their support and guidance.

I would also like to express great appreciation for the Signal Integrity group at Amphenol-TCS for the opportunity to work on this project.

TABLE OF CONTENTS

DEDICATION	iv
ACKNOWLEDGEMENTS	v
TABLE OF CONTENTS.....	vi
LIST OF FIGURES.....	ix
LIST OF TABLES	xiii
ABSTRACT.....	xv
CHAPTER 1: INTRODUCTION	1
1.1 Background.....	1
1.2 Signaling Modes of Differential Pairs	3
1.3 Twinaxial Cable Structure.....	4
1.4 Measurement	5
1.5 Simulation Methods	6
1.6 Literature Review.....	7
1.7 Proposed Estimate of the Resonant Frequency	9
1.8 Measurement and Simulation Analysis.....	10
1.9 Organization	10
CHAPTER 2: FIXTURING AND CALIBRATION	12
2.1 Device Under Test	12
2.2 Test Fixture.....	15
2.3 Commercial Twinaxial Cable	17
2.4 Frequency Domain Equipment, Calibration, and Limitations.....	18
CHAPTER 3: MEASUREMENTS	21

3.1 Frequency Domain Measurements: Commercial Twinaxial Cables	21
3.2 Frequency Domain Measurements: Experimental Twinaxial Structures.....	24
3.3 Results	37
CHAPTER 4: COMPUTER SIMULATION.....	41
4.1 Full-Wave Simulation Tool.....	41
4.2 Full-Wave Modeling and Simulation Technique	41
4.3 Full-Wave Simulation Results.....	45
4.4 Circuit Model and Analysis Results	49
CHAPTER 5: Discussion of Results	54
5.1 Frequency Domain Comparison	54
5.2 Summary	61
CHAPTER 6: Conclusions and Future Work	66
6.1 Measurements and Fixturing	66
6.2 Full-Wave Simulation	68
6.3 Circuit Analysis	69
6.3 Conclusions	69
6.4 Future Work.....	70
APPENDICES.....	72
APPENDIX A: Semi-Rigid Coaxial Cable Description.....	73
APPENDIX B: Commercial Twin Axial Data Sheet	75
APPENDIX C: Turn Length Calculation	76
APPENDIX D: Quasi-Static Simulation Tool Detail	77
APPENDIX E: Circuit Models	79

LIST OF REFERENCES.....	81
-------------------------	----

LIST OF FIGURES

Figure 1: Twinaxial Cable Cross-Section	1
Figure 2: Differential Transmission, Commercial Twinaxial Cable	2
Figure 3: Cross-section, Commercial Twinaxial Cable Assembly	4
Figure 4: CAD drawing of DUT	12
Figure 5: Isometric view CAD drawing of DUT	13
Figure 6: S_{DD21} , DUT and Commercial Twinaxial Cable	14
Figure 7: Commercial Cable	14
Figure 8: DUT Cable	14
Figure 9: Isometric view of CAD drawing of test vehicle assembly	15
Figure 10: Free-body diagram of test vehicle assembly with DUT	16
Figure 11: Commercial Twinaxial Cable Termination.....	17
Figure 12: Agilent 4-port VNA.....	18
Figure 13: DUT connected to the VNA.....	18
Figure 14: Agilent Electronic Calibration module connected to the VNA.....	19
Figure 15: S_{DD21} , Commercial Twinaxial cable, Three Lengths.....	21
Figure 16: S_{DD21} , Commercial Twinaxial Cable, Longitudinal vs. Spiral Shield	22
Figure 17: S_{DD21} , Commercial Twinaxial Cable, Drain Wire vs. No Drain Wire.....	23
Figure 18: Experimental Test Vehicle and DUT	24
Figure 19: Shield Connection with Solder.....	24
Figure 20: Isometric View of 30 AWG Wire Applied as the Shield to the DUT	25
Figure 21: DUT With Spirally Wrapped Foil Applied as the Shielding Structure	26
Figure 22: Center frequency calculation of the resonant behavior in a transmission	28

Figure 23: S_{DD21} , DUT , No Shielding vs. Longitudinally Wrapped Copper Foil Shield	.29
Figure 24: S_{DD21} , DUT, Spiral 30 AWG Shields	30
Figure 25: S_{DD21} , DUT, Spiral 30 AWG shields, 10% Turn Spacing Variance	31
Figure 26: S_{DD21} , DUT, Varying Spiral Shield Geometry	32
Figure 27: S_{DD21} , DUT, Varying Shield Material	33
Figure 28: S_{DD21} , DUT, Spiral Copper Foil Shields	34
Figure 29: S_{DD21} , DUT, Spiral Aluminized Polyester Shields	35
Figure 30: S_{DD21} , DUT, Spiral Aluminized Polyester Shields, 10% Turn Spacing Variance	36
Figure 31: Transmission Line Circuit Model	37
Figure 32: Simulated Twinaxial Structure	43
Figure 33: S_{DD21} , Full-Wave Simulation, Solid Shield	45
Figure 34: S_{DD21} , Full-Wave Simulation, 30 AWG Spiral Shields	46
Figure 35, Full-Wave Simulation, Varying Tightness Factor	47
Figure 36: Equivalent Circuit Model of a Two Conductor Lossless Transmission Line	49
Figure 37: 3D Model of the Twinaxial Transmission Line Structure	50
Figure 38: Cross-Section, First π Network Segment	50
Figure 39: Cross-Section, Third π Network Segment	50
Figure 40: Cross-Section, Second π Network Segment	50
Figure 41: Cross-Section, Fourth π Network Segment	50
Figure 42: Equivalent Circuit Model for One Turn Spacing of a Twinaxial Structure	51
Figure 43: SPICE AC Analysis Results, Equivalent Circuit Models of Twinaxial Structures	53

Figure 44: S_{DD21} , Method Comparison, 1.200in. Turn Spacing.....	55
Figure 45: S_{DD21} , Method Comparison, 0.649in. Turn Spacing.....	56
Figure 46: S_{DD21} , Method Comparison, 0.590in. Turn Spacing.....	57
Figure 47: S_{DD21} , Method Comparison, 0.530in. Turn Spacing.....	58
Figure 48: S_{DD21} , Method Comparison, 0.270in. Turn Spacing.....	59
Figure 49: S_{DD21} , Commercial Twinaxial Cable, 0.270in. Turn Spacing.....	60
Figure 50: Measured Resonance vs. Predicted Resonance, 30 AWG Spiral Shields	61
Figure 51: Measured Resonance vs. Predicted Resonance, 0.200in. Wide (<i>Width A</i>) Aluminized Polyester Spiral Shields	62
Figure 52: Full-Wave Simulated Resonance vs. Predicted Resonance, 30 AWG Spiral Shields	63
Figure 53: AC Analysis Resonance vs. Predicted Resonance, 30 AWG Spiral Shields...	64
Figure A 1: Mechanical Drawing of Female SMA Interconnect.....	73
Figure A 2: Semi-rigid Coaxial Transmission Line Datasheet	74
Figure B 1: Data Sheet for a Commercially Available Twinaxial Cable Assembly.....	75
Figure C 1: Top view of one turn spacing	76
Figure E 1: Circuit Model, Twinaxial Structure, 30 AWG Spiral Shield, Turn Spacing of 1.200in.....	79

Figure E 2: Circuit Model, Twinaxial Structure, 30 AWG Spiral Shield, Turn Spacing of 0.649in.....	79
Figure E 3: Circuit Model, Twinaxial Structure, 30 AWG Spiral Shield, Turn Spacing of 0.590in.....	80
Figure E 4: Circuit Model, Twinaxial Structure, 30 AWG Spiral Shield, Turn Spacing of 0.530in.....	80
Figure E 5: Circuit Model, Twinaxial Structure, 30 AWG Spiral Shield, Turn Spacing of 0.270in.....	80

LIST OF TABLES

Table 1: Experimental DUT shield configurations, 30 AWG	27
Table 2: Measurement Results, DUT, 30 AWG Spiral Shield	39
Table 3: Measurement Results, DUT, 0.200in. Copper Foil Spiral Shield	39
Table 4: Measurement Results, Constant Turn Spacing, Varying Spiral Shield Geometry	39
Table 5: Measurement Results, DUT, Aluminized Polyester Spiral Shield	40
Table 6: Full-wave Simulation Case Details.....	44
Table 7: Full-wave Simulation Results, Twinaxial Structures	48
Table 8: Full-wave Simulation Results, Twinaxial Structures, Varying Tightness Factor	48
Table 9: SPICE AC Analysis Results, Equivalent Circuit Models for Twinaxial Structures	53
Table 10: Magnitude of Center Frequency Variance Calculated From Equation 3	65
Table 11: % Deviation Measured vs. Predicted Resonance Frequencies for Aluminized Polyester Shields.....	66
Table 12: % Deviation Measured vs. Predicted Resonance Frequencies for 30 AWG Shields	67
Table 13: % Deviation Simulated vs. Predicted Resonance Frequencies for Full-Wave Simulations	68
Table 14: % Deviation Simulated vs. Predicted Resonance Frequencies for Circuit Analyses	69

Table 15: Measurement and Simulation Results Compared to the Predicted Resonance for
30 AWG shields.....70

ABSTRACT

AN INVESTIGATION ON THE RESONANCE OBSERVED IN A SPIRALLY SHIELDED TWINAXIAL DIFFERENTIAL PAIR

by

David Richard Levine

University of New Hampshire, December 2012

Spirally shielded twinaxial cable assemblies are extensively used in multi-gigabit-per-second digital telecommunications systems. Unlike ideally shielded Twinaxial cables, spirally shielded cables exhibit resonant behavior which limits system throughput.

This body of work illustrates a predictive method for determining resonant behavior in twinaxial cables through physical measurement of commercially available cables and analogous transmission line fixtures, full-wave and quasi-static simulations, and equivalent circuit analysis.

It will be shown that frequency dependent standing wave resonances in twinaxial cables are independent of cable length and dependent on cross-sectional feature sizes, dielectric properties, and spiral shield pitch.

CHAPTER 1: INTRODUCTION

In this chapter, a background description of twinaxial cables and their application are detailed. The chapter highlights the motivation for the examination of the twinaxial cable with a focus on shielding practices used in commercial cable construction. The chapter describes different modes of propagation in a differential pair such as a twinaxial cable. The chapter details the experimental structure used in measurement, the measurements performed on the described structure, simulation models, and methodologies used in the analysis.

1.1 Background

Unshielded twisted pair cables were traditionally used for digital data transmission at low bit rates. To satisfy demand for higher bit rate transmission, twinaxial cables consisting of a pair of signal wires with a conductive shield were developed to shield the signal more effectively. To further improve performance, a ground drain wire was added. Due to the imperfect current balance of the differential lines, there was a loss at higher data rates from energy leakage. To mitigate the imbalanced effects of the lines and improve performance, a conductor was introduced as a shield (see Figure 1). This shielding also lowered the transmission line's susceptibility to electromagnetic interference from outside sources.

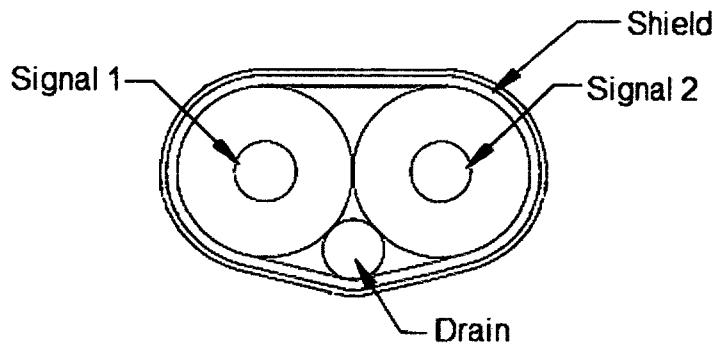


Figure 1: Twinaxial Cable Cross-Section

Contemporary twinaxial cables using the above configuration are utilized in digital communications channels such as Small Form-factor Pluggable (SFP) based interconnect applications. These applications commonly use a 10 gigabit-per-second (GBps) data rate, with future needs exceeding this rate [Zha11].

Twinaxial cables are commonly shielded with a spirally wrapped conductor. Spiral wrapping increases mechanical strength over other wrapping methods such as longitudinal wrapping. However these spirally shielded twinaxial cables used in multi-gigabit-per-second digital telecommunications equipment resonate at frequencies greater than 5 GHz (Figure 2).

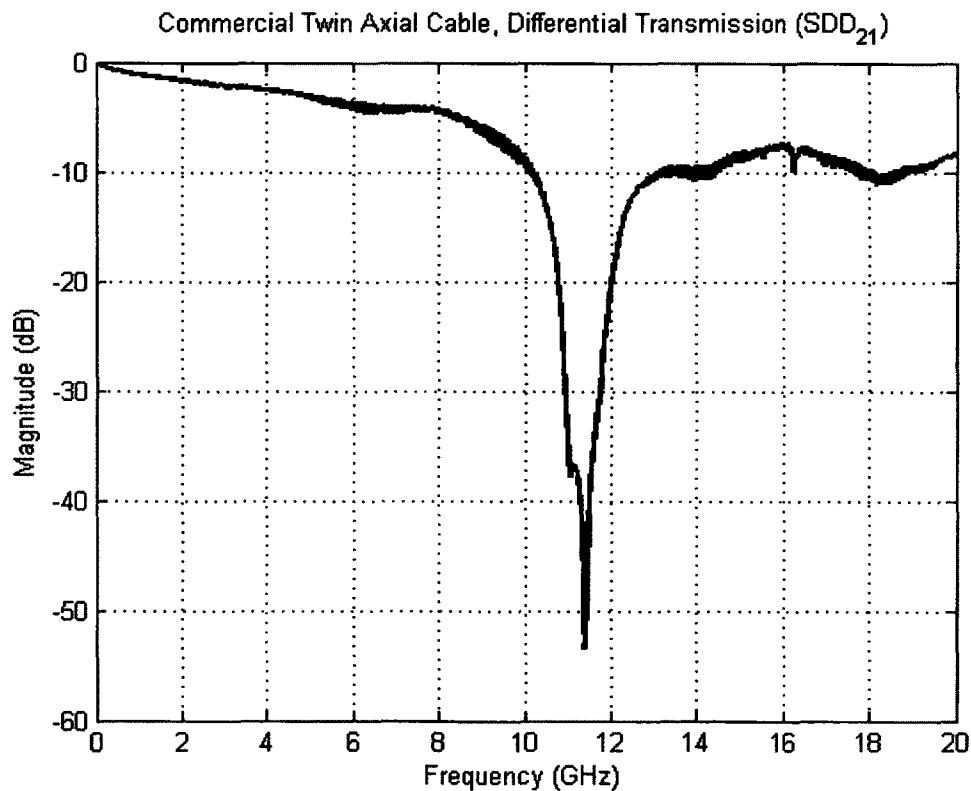


Figure 2: Differential Transmission, Commercial Twinaxial Cable

In this thesis the effects of spiral shielding on twinaxial cables will be investigated through suitable experiments. Simulations and equivalent circuit analyses of the twinaxial cables will also be used to predict the resonant frequency.

1.2 Signaling Modes of Differential Pairs

Differential signal pairs with conductive shielding consist of three separate conductors, two signal conductors of the same material with the same diameter and the third conductor, a shield on the dielectric casing of the signal conductors. The currents in a differential twinaxial cable system are ideally assumed to be balanced. However a slight imbalance of currents typically occurs. This imbalance may be due to the imperfect transmitting and receiving packages and mode conversions. In such a case, twinaxial cable currents can be split into two components: a differential mode (odd mode), and the common mode (even mode) [Bog10]. The odd mode induces no net current in the shield system as each of the two signal conductors act as the return path for its complement while the even mode induces current flow on the shield. The odd-mode impedance of the transmission line is the impedance between one individual signal line and the ground or return path, when the signal lines are oppositely excited. The differential impedance between the two signal lines of the transmission line is twice the odd mode impedance.

Even-mode signaling on a differential transmission line is equivalent to driving both signal lines with identical excitations. Even-mode impedance is the characteristic impedance of one signal line as a common signal propagates through the pair. Common-

mode impedance is half of the even-mode impedance as the common-mode signals can be considered as a pair of parallel transmission lines.

Asymmetrical features of the driving systems, interconnects, and transmission line can cause mode conversion, or the conversion of a differential signal to a common-mode signal. Mode conversion in a system increases current flow on the return path and can induce electro-magnetic interference (EMI) issues with surrounding systems. This phenomenon is examined in this thesis through measurement and simulation.

1.3 Twinaxial Cable Structure

In a twinaxial cable the signal conductors vary from 24 (0.0201 inches) to 30 (0.0100 inches) AWG. Dielectric properties and feature sizes typically provide a differential characteristic impedance of 100-ohms. A cross-section of a typical two-pair twinaxial cable assembly can be seen in Figure 3.

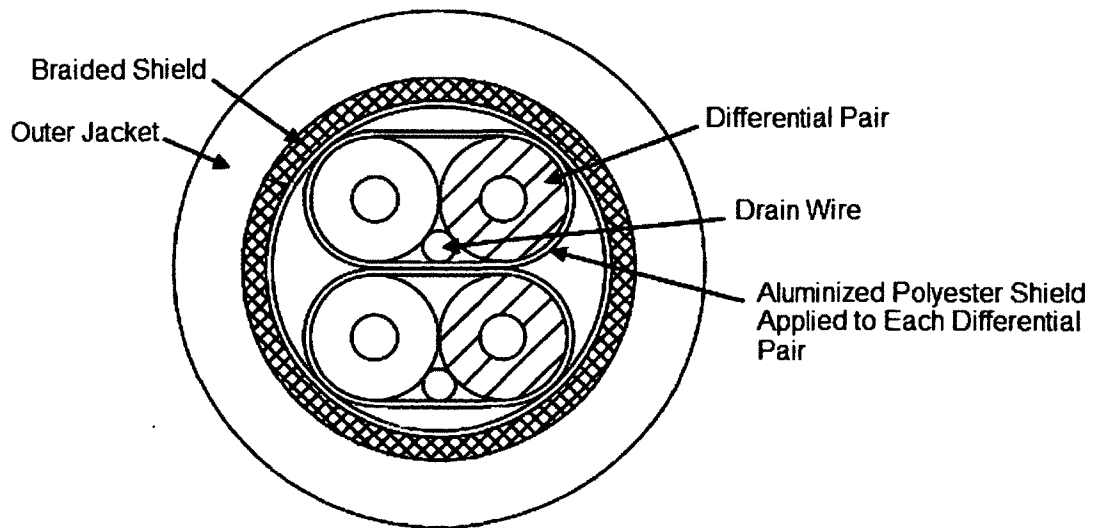


Figure 3: Cross-section, Commercial Twinaxial Cable Assembly

A typical measured commercial twinaxial cable is composed of two 0.0201 inch signal conductors enveloped in a polyolefin foam dielectric of outside diameter 0.056 inches, whose relative dielectric constant (ϵ_r) is 1.65, and loss tangent is 0.00045. Encompassing each signal pair and drain wire is a spiral shield composed of 0.001 inch aluminized polyester foil. A typical differential characteristic impedance of such a cable is 100-ohms. Commercial cables commonly package multiple differential pairs into a cable assembly. Braided conductor is used to isolate differential pairs from outside interference sources, and the assembly has a polyvinyl-chloride (PVC) jacket. A data sheet for the tested commercial twinaxial cable is provided in Figure B 1, APPENDIX B.

1.4 Measurement

To understand the impact of twinaxial cable shielding methods on system performance, frequency domain data were collected both on commercial twinaxial cable samples and a specially constructed cable device in an experimental fixture. The experimental fixture will be able to furnish additional data as the shielding configuration can be varied. The fixture consists of an experimental twinaxial cable and a support structure.

Scattering parameters (S-parameters) provide a means for analyzing the electrical characteristics of a distributed network in the frequency domain [Kur65]. Though originally defined for single-ended networks, S-parameters have been adapted for differential networks. S-parameter data on the device-under-test (DUT) were collected with an Agilent Vector Network Analyzer (VNA). This instrument is a single-ended precision 4-port, 50GHz unit interfaced with Agilent's proprietary Physical Layer Test System (PLTS) software. Differential S-parameters are mathematically calculated from

the single-ended measurements. Electronic calibration (ECal) is performed prior to measurement sessions, placing the reference plane at the end of the VNA coaxial cables. In the frequency range of 10MHz to 20GHz, odd and even mode transmission and reflection is provided by the S-parameter data. Only the differential S-parameters are used in this study as they are S_{DD21} , where the 'D' corresponds to differential mode sources/destinations, the first numeral is the destination port, and the second is the source port.

1.5 Simulation Methods

Many software packages are available for simulating and predicting electrical performance of transmission line structures. In this study the simulations were performed using the Finite Integral Technique (FIT) in the Computer Simulation Technology (CST) Microwave StudioTM software package, a time-domain solver [Sch96]. CST discretizes modeled structures into hexahedral blocks, and proceeds to solve for the integral form of Maxwell's equations. Electric voltages are allocated along the edge of discretized hexahedrals, while magnetic voltages are allocated along edges between centers of the discretized hexahedrals.

Twinaxial cables with helical shielding systems are geometrically complex, and include spiral structures with complex multi-dimensional edges along other model members. This can introduce additional sources of error especially with a hexahedral meshing scheme. Approximations of actual physical DUTs were modeled in the software environment to facilitate discretization of all geometric features. Models considered are twinaxial cables and are analogues to experimental DUTs measured in this thesis. These models are considered ideal and do not include end effects.

An equivalent circuit model of a twinaxial cable was developed to provide transmission data, which were compared to the results of the full-wave simulations and the measured experiments. Circuit parameters were computed with quasi-static solver tools. A circuit simulation program (National Instruments Multisim™) was used to perform analysis of the circuit model.

1.6 Literature Review

Numerical methods employing full-wave Finite Element Analysis have been used to model and characterize the effect of the spiral shield on twinaxial cables. D.N. de Araujo et al. [Ara08] presents this method using Ansoft's High Frequency Structure Simulator™ (HFSS) software and compares computation results of different configurations of the twinaxial cable's spiral shield. This approach differs from the full-wave time-domain simulation method utilized in the present thesis by computing the S-parameters in the frequency domain. Araujo et al. make the assumption that the overlapping of the spiral shield can be represented by a gap in the shield, as these are both discontinuities in the current's return path. Araujo et al. conjecture that the periodicity of the discontinuity in the twinaxial cable's shield is the cause for the filtering effects of the cable, and a lower pitched spiral gap increases the center frequency of the resonant notch. From his simulated results he claims that as the length of the cable increases, the resonant notch's 'q-factor' increases, as attenuation is proportional to the number of turns in the spiral shield.

Two theoretical resonance mitigation techniques presented in his paper are as follows: the first consists of a dual drain wire design which will reduce the attenuation in the resonant notch of the twinaxial cable as this lowers the magnitude of current flowing

on the shield. The second mitigation technique presented is a twist-synchronous design, where the entire single-drain wire twinaxial cable is twisted helically.

Limitations of this paper include lack of correlation to measurement of a physical DUT, lack of correlation to an analytic model, and erroneous assumptions regarding longer (~10m) cable lengths. Cable length and resonance center frequency have not been decoupled in this paper. To simplify and reduce the computational effort involved in modeling and analyzing longer cable lengths, smaller sections of cable have been simulated and cascaded in a system level simulation. The assumption that this approach is equivalent to one long cable segment is invalid due to the additional boundaries imposed in the model. Any effects of the end conditions imposed by the boundaries will be distributed at multiple places throughout the concatenated model, yielding a different result than a solid long transmission line simulation.

Matsumoto et al. [Mat10] developed an equivalent circuit model for the simulation of filters formed on printed circuit boards. The filters examined in this study are periodic perturbations in the ground plane return path of the microstrip transmission line structure in the form of “I” and “L” shaped slits. A design decision was made to use transmission line model segments (distributed-element) in lieu of lumped-element analysis. Matsumoto et al. based this decision on the lack of existing equations that describe the inductances and capacitances based on the feature sizes of the slits. Since transmission line structures can adequately express physical parameters of the slit structures, these were chosen as the components for the circuit model. Electromagnetic coupling between the microstrip transmission line and the slit transmission line structure

was chosen to be an ideal transformer in the model. Ideal transformers are also included in the model to electromagnetically couple between slits.

Matsumoto et al. compared S-Parameter results garnered from simulating the microstrip structures in a full-wave simulation package and from quasi-static circuit simulation. Full-wave simulation results agree closely with quasi-static circuit simulation results for the prediction of the first resonance (f_0). The full-wave results contain more detail as frequency increases. Matsumoto et al. explain that the errors are caused by dispersion of the dielectric permittivity in the simulation package used.

Simulations and results obtained by Matsumoto et al. show that there is validity to creating quasi-static circuit models for periodic filter elements in the return path of a transmission line. The inadequacies of lumped-element representations of the transmission line structures examined in this paper can be minimized by the utilization of 2D quasi-static tools to calculate the lumped-element parameters. This paper provides the motivation in my analysis of twinaxial Cables to model the differential center conductors as a differential transmission line while the spiral shield can be considered as a periodic filter structure.

1.7 Proposed Estimate of the Resonant Frequency

At the resonance, as there is minimal transmitted power, because the incident and the reflected waves destructively interfere which results in a standing wave at that frequency. We have observed that the wavelength at the resonant minimum in the transmission of spirally shielded twinaxial cables is related to a turn length of the spiral wrap and the propagation constant of the transmission line. The length of one turn is half the wavelength at the resonance frequency. The accuracy of this predictive equation will

be checked with calibrated measurements and simulations. The frequency at resonance is given by Equation 1, where V_p is the phase velocity of the transmission line, and l is the unwrapped length of one turn of the spiral shield.

$$f_{res} = \frac{V_p}{2l} \quad [1]$$

1.8 Measurement and Simulation Analysis

The accuracy of the DUT was assessed by comparing the measured data from this structure to the data obtained using commercially produced twinaxial cables. Results from full-wave simulations are used to validate experimental results. Equivalent circuit analysis was assessed through comparison to experimental and full-wave results. The proposed predictive equation's accuracy and range of application was checked by comparing the predicted results to measurement, simulation, and the equivalent circuit analyses.

1.9 Organization

Chapter II describes the techniques used to acquire the data with the experimentally designed cable fixture and the commercial twinaxial cables. Calibration methods and error sources present in the measurement are also discussed. This chapter will also detail the design and construction of the experimental cable fixture. Chapter III presents measurements in the frequency domain for the experimental structure and twinaxial cables. Chapter IV details full-wave simulation methodologies and the techniques used in modeling the experimental structure analog and twinaxial cable analog and the techniques and results based on circuit analysis of twinaxial cable structures.

Chapter V presents the results and a detailed analysis of modeling and simulation work. Results from measurement and simulation are compared with the proposed resonance mechanism equation. Chapter VI presents conclusions based upon analysis, and presents suggestions for future work in the topic.

CHAPTER 2: FIXTURING AND CALIBRATION

In this chapter, the device under test (DUT) and the test fixture used in measuring the device under test are defined and detailed. Design and fabrication of both structures is presented within this chapter. Termination techniques and measurement techniques for collecting data on commercial twinaxial cables is shown. In this chapter emphasis is also placed upon the calibration techniques used and the motivation for calibration.

2.1 Device Under Test

The resonance phenomenon under study has been observed only in spirally shielded cable. Modification of the pitch of the spiral shield is necessary to study its effect on the frequency response of the twinaxial cable. Since it is difficult to modify the physical structure in commercially available twinaxial cables, a scaled device which allows modification of the spiral geometry of the shielding system has been used to study this phenomenon.

The device (shown in Figure 4) used for this experiment consisted of a 9.0 inch long multi-conductor transmission line constructed from two pieces of 0.02 inch diameter silver plated copper wire (9.0 inches in length) coated with polyethylene.

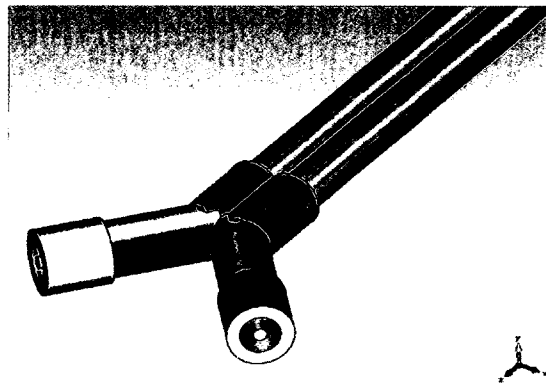


Figure 4: CAD drawing of DUT

The center-to-center distance between the signal conductors is 0.065 inches. These feature sizes were chosen to yield a differential impedance compatible with the 100-ohm (differential) environment of the measurement equipment. The device under test (DUT) did not include a ground drain wire. To connect the test equipment to the DUT, a rigid termination was designed with female a subminiature version A (SMA) interconnect for the signal launches. As this structure is not rigid during the application of shielding and data collection, an additional test fixture was built to compensate for this instability. An isometric view cross-section of the DUT is provided in Figure 5.

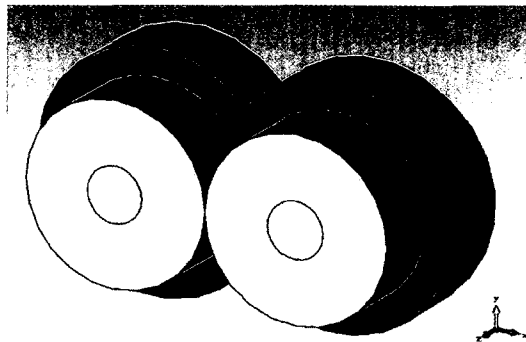


Figure 5: Isometric view CAD drawing of DUT

Examples of differential transmissions (insertion losses) through the DUT transmission line and a commercially produced twinaxial cable are shown in Figure 6. The commercial twinaxial cable (Figure 7) has overlap in the conductive ribbon spiral shield and a drain wire, while the DUT-based experiment has 0.270 inch gaps in the spiral shield, which consists of a 30 AWG wire (Figure 8).

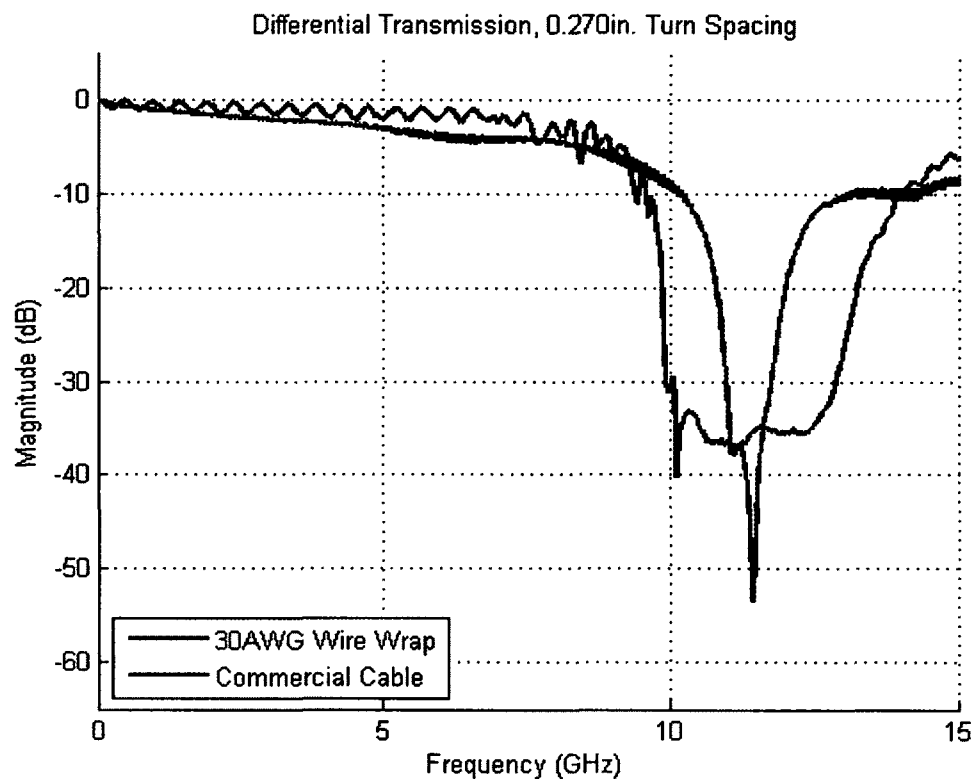


Figure 6: S_{DD21} , DUT and Commercial Twinaxial Cable



Figure 7: Commercial Cable

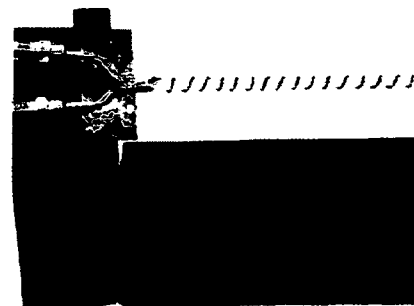


Figure 8: DUT Cable

2.2 Test Fixture

To provide electrically repeatable results, a test fixture was designed (Figure 9).

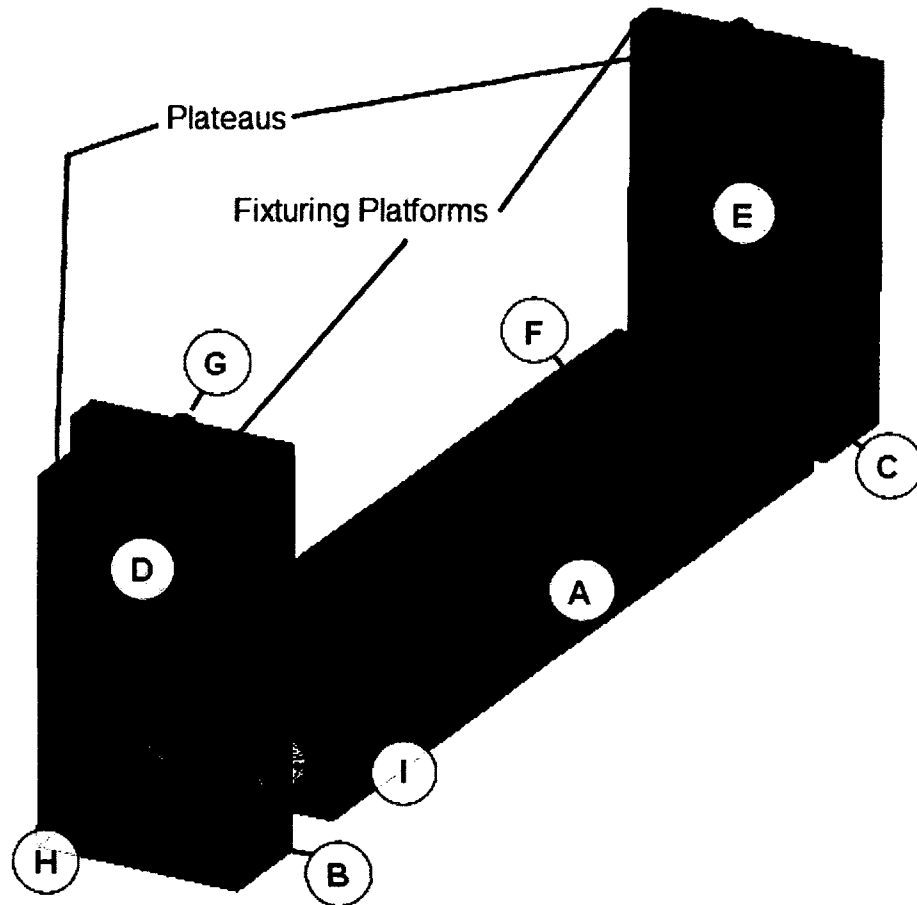


Figure 9: Isometric view of CAD drawing of test vehicle assembly

The test fixturing used in this series of experiments was designed to avoid additional impedance discontinuities by being mechanically rigid and electrically inert. The test vehicle was constructed out of 1.0 inch thick Polyoxymethylene (POM), a hard machinable plastic. The base (part A in Figure 9) of the test vehicle was chosen to accommodate the length of the DUT (9.0 inches). The width of the base was chosen to provide ample clearance for all assembly screws and dowels (2.0 inches). One end of the

base was machined to accept two 0.3125 inch, 24 threads per inch (TPI), screws (part C in Figure 9), while the opposite end was milled and reamed to accept two 0.375 inch steel dowels (part B in Figure 9). Springs (part I) were placed over part B to apply controlled force to the DUT spanning the two upright members. The screw (part H) and spring combination provides a mechanism for applying a force along the Z-axis which places the DUT under tension. A free-body diagram of the experimental setup is provided in Figure 10. The test vehicle's two vertical members are not identical; each has been machined to a depth of 0.375 inches with an end mill to create a plateau. Three retention holes were drilled and tapped to accommodate 8x32 machine screws (part G in Figure 9). The height of each of the fixturing platforms was 4 inches, while the lower tier's height was machined to 3.75 inches in height. Part D in Figure 9 was machined and counter-bored to pass through two 0.375 inch steel dowels (part B) and one 0.375 inch screw (part H), the second (part E in Figure 9) was machined to accept a centered 0.5 inch dowel (part F in Figure 9) and two 0.375 inch steel dowels (part C in Figure 9).

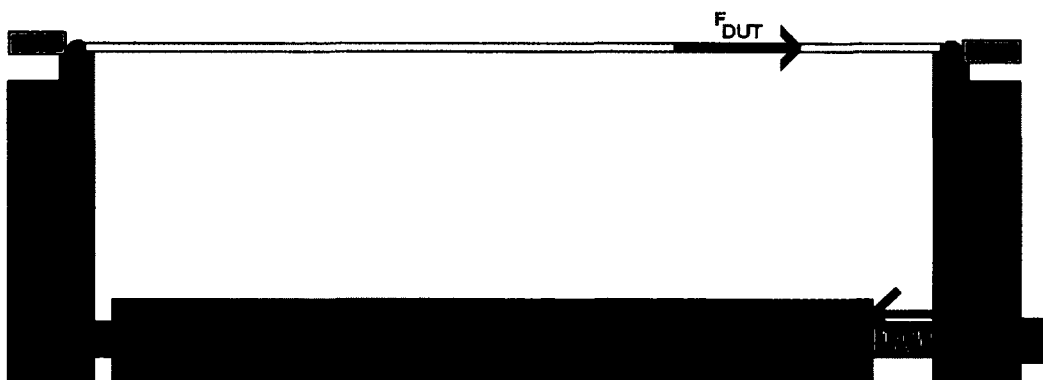


Figure 10: Free-body diagram of test vehicle assembly with DUT

2.3 Commercial Twinaxial Cable

Frequency domain data were collected from terminated twinaxial cable structures. To verify that the spirally-wrapped shield imparts a resonance on a differential transmission line, a cable with a longitudinally applied shield was measured. Three different lengths (40.16 inch, 56.69 inch, and 68.50 inch) of identically-cross-sectioned spirally-shielded cable were used to measure the impact of length upon the resonance frequency. Assessing the effect of a ground drain wire on the resonance frequency was accomplished by measuring a twinaxial cable without a ground drain wire.

Termination of these commercial cables (Figure 11) is critical in collection of data. Poor termination will cause many effects such as high magnitude reflections. Care was taken in the cable termination process to help mitigate unwanted effects.

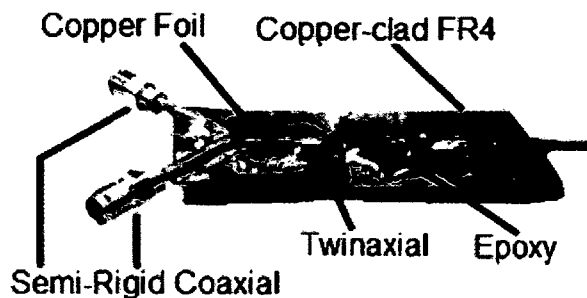


Figure 11: Commercial Twinaxial Cable Termination

Cable terminations were done by first removing the outside jacketing and conductive mesh shielding layers and then removing 0.150 inches of aluminized polyester spiral shield to expose the dielectric-coated signal conductors and ground drain wire. Signal conductors were then electrically coupled to 1.0 inch lengths of 50-ohm semi-rigid coaxial cable. Copper-clad FR4 (glass weave and epoxy based dielectric) was

used as the ground system for the termination. The drain wire was fixed to the copper-clad FR4 along with each semi-rigid coaxial cable length. Copper foil was then used to shield the exposed signal conductors and control impedance. A two-part epoxy was used for mechanical stability as a strain relief.

2.4 Frequency Domain Equipment, Calibration, and Limitations

All measurements were performed at Amphenol-TCS's Nashua facility. An Agilent Technologies PNA series 4-port vector network analyzer (VNA) was used to collect frequency domain data (Figure 12).

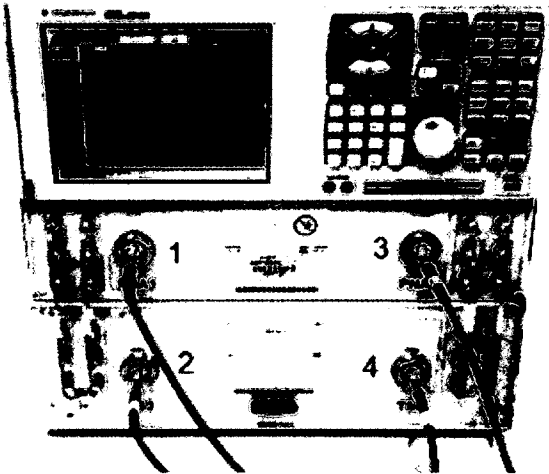


Figure 12: Agilent 4-port VNA

This instrument measures the incident and reflected voltages and currents in a 4-port network DUT. The DUT connected to the VNA is shown in Figure 13.

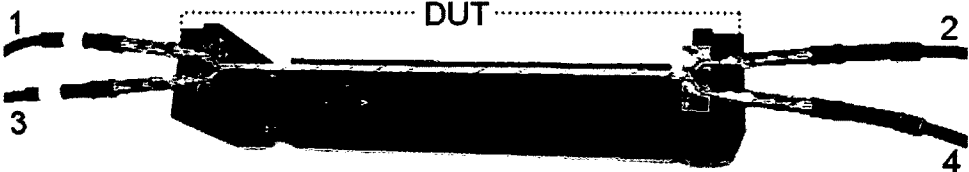


Figure 13: DUT connected to the VNA

Prior to the collection of frequency domain data the vector network analyzer was calibrated using Agilent's Electronic Calibration. This calibration technique places the measurement plane at the end of the test cables and does not compensate for any fixture launches or connectors. Placing the measurement plane at this point in space compensates for mismatch in the driving hardware of the vector network analyzer and the test cabling. Electronic calibration modules contain known S-parameter data, and calculate the error terms of the instrument based upon traceable and verifiable standards [Agi12]. The measured value of this standard is then compared to the calibrated value of the standard. For this series of measurements, electronic calibrations were performed from 10 MHz to 20 GHz. The setup used to calibrate the VNA with the Agilent electronic calibration module is illustrated in Figure 14.

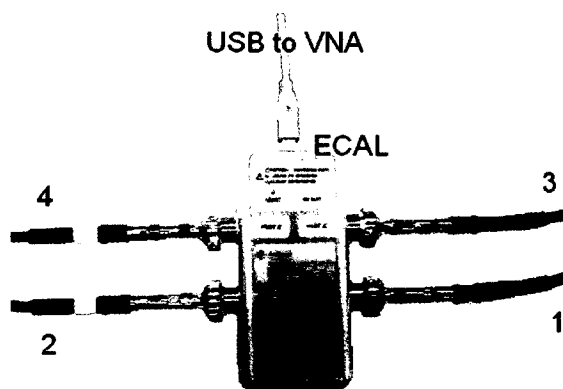


Figure 14: Agilent Electronic Calibration module connected to the VNA

Since electronic calibration was employed, termination end-effects of the DUT are included in all frequency-domain measurements. A commonality between all DUT structures' terminations is that they are not ideally matched in impedance to the measurement cables, nor to the shielded transmission line segment of the DUT.

Impedance discontinuities present in DUT configurations cause the coefficient of reflection to be non-zero.

CHAPTER 3: MEASUREMENTS

Chapter 3 details the measurements collected on the two twinaxial analogous structures and the commercially available twinaxial cables detailed in Chapter Two. This chapter defines the shielding configurations applied to each DUT. The chapter highlights the test equipment and measurement techniques utilized in the frequency domain analysis of twinaxial analogous structures and commercially available twinaxial cables, providing four port scattering parameters of these differential transmission line structures.

3.1 Frequency Domain Measurements: Commercial Twinaxial Cables

The calibrated vector network analyzer measurements of S_{DD21} for identically cross-sectioned, spirally-shielded, commercially available twinaxial cables are shown in Figure 15 for three lengths: 40.2 inches, 56.7 inches, and 68.5 inches.

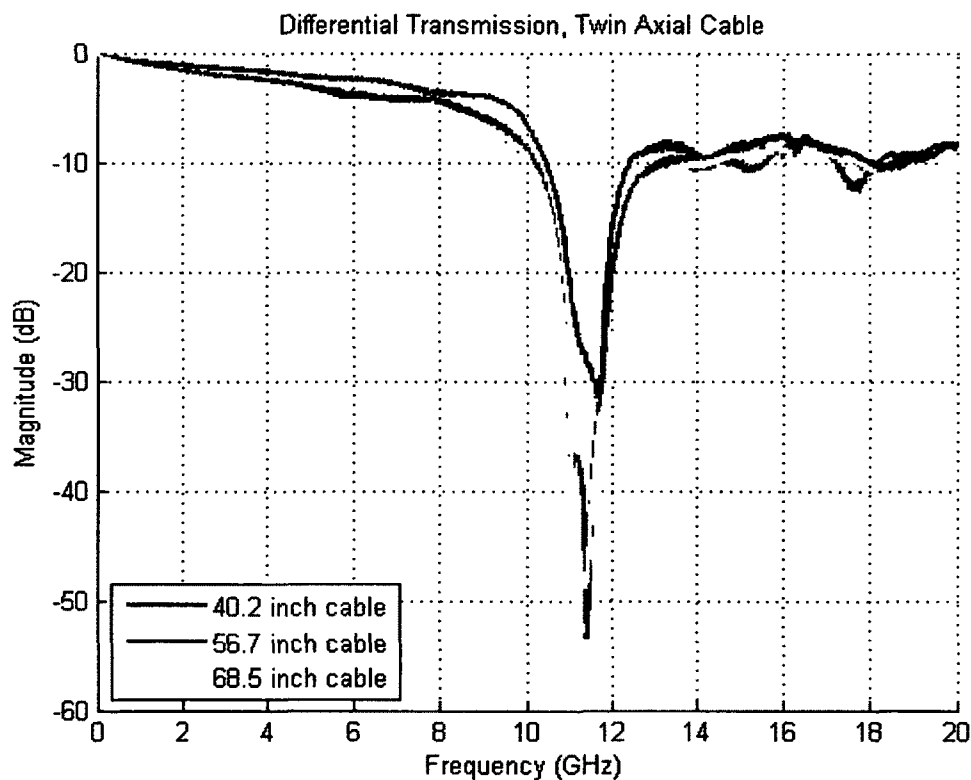


Figure 15: S_{DD21} , Commercial Twinaxial cable, Three Lengths

The cable consists of two 24AWG solid silver plated copper signal conductors inside a 0.056in diameter foam polyolefin dielectric ($\epsilon_r=1.65$) with a 27 AWG solid tinned copper ground drain wire, and a 0.001in aluminized polyester foil shielding. This shield is wrapped with a 20% overlap. All three lengths of cable resonated at 11.4GHz.

The measured differential transmission, S_{DD21} , of a longitudinally shielded commercial twinaxial cable and a spirally shielded twinaxial cable of similar length is shown in Figure 16. There is no resonance measured in the longitudinally shielded cable sample, while the spirally shielded cable exhibits a resonance 11.4GHz.

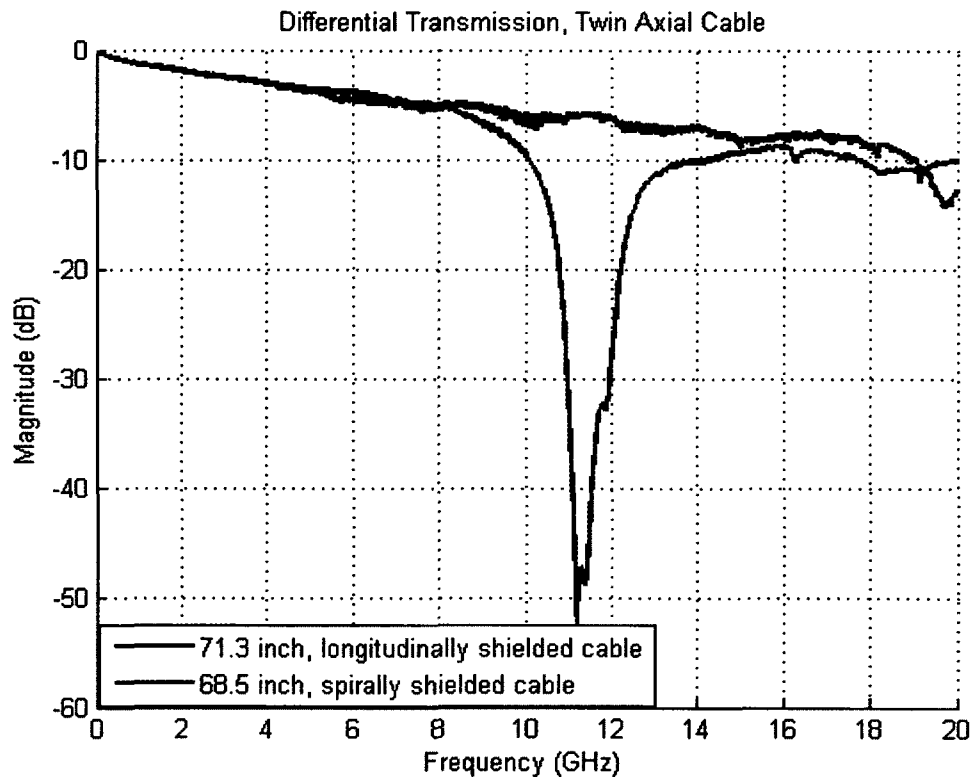


Figure 16: S_{DD21} , Commercial Twinaxial Cable, Longitudinal vs. Spiral Shield

Figure 17 illustrates the differential transmissions of spirally wrapped twinaxial cables, with the ground drain wire removed from one sample. Both cables were created from the same cable sample. In comparison, the resonant phenomenon center frequency moved 300MHz lower when there is no drain wire, compared to a cable with a drain wire. Prior to the resonance, the cable without a drain wire exhibits more natural losses, even though it is of shorter length.

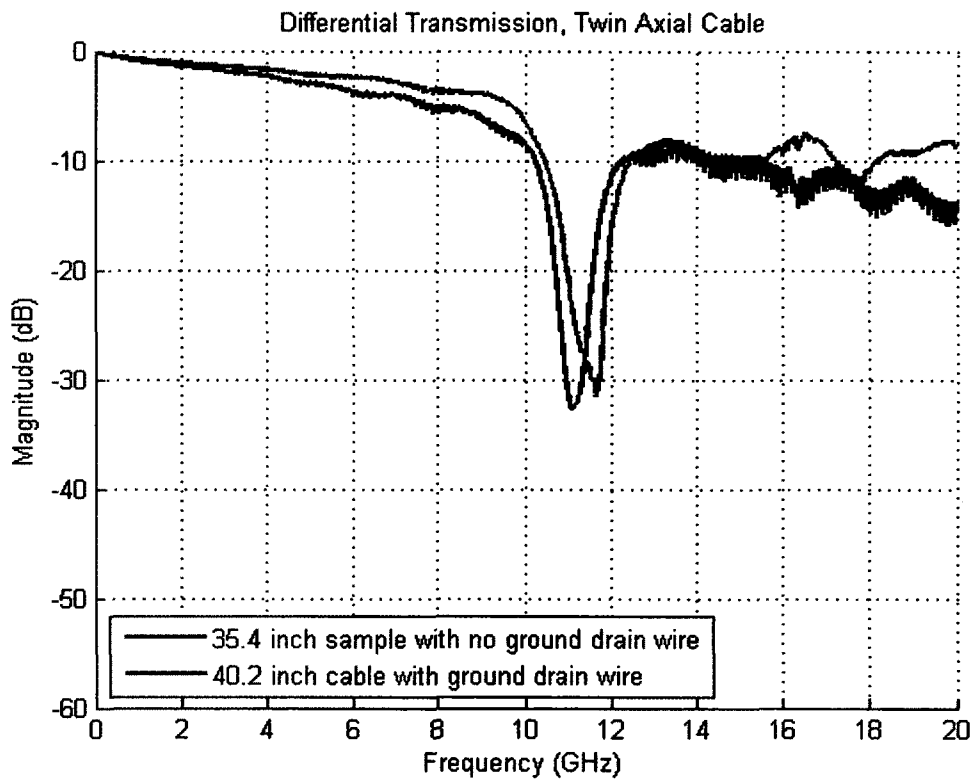


Figure 17: S_{DD21} , Commercial Twinaxial Cable, Drain Wire vs. No Drain Wire

3.2 Frequency Domain Measurements: Experimental Twinaxial Structures

Figure 18 shows the test fixture with no shielding applied. The DUT in this series of measurements is considered as one differential pair with no ground drain wire. Unshielded measurements were collected to create a baseline for comparing shielding effectiveness of subsequent DUT shielding configurations. In each experimental case where a shield is applied, it has been connected between each termination of the DUT via a solder connection (Figure 19). This establishes a return reference between each end of the transmission line and ensures electrical continuity in the shield from end to end.

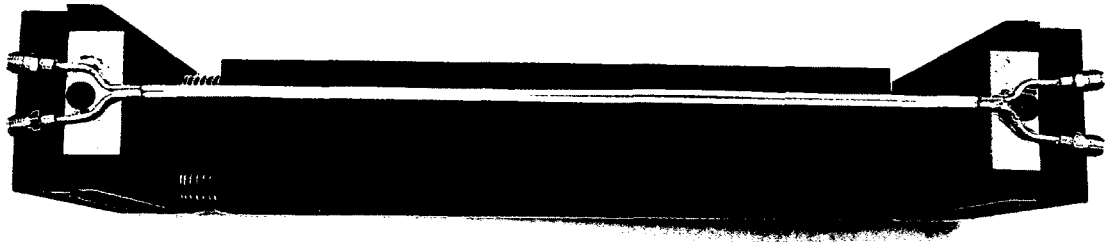


Figure 18: Experimental Test Vehicle and DUT

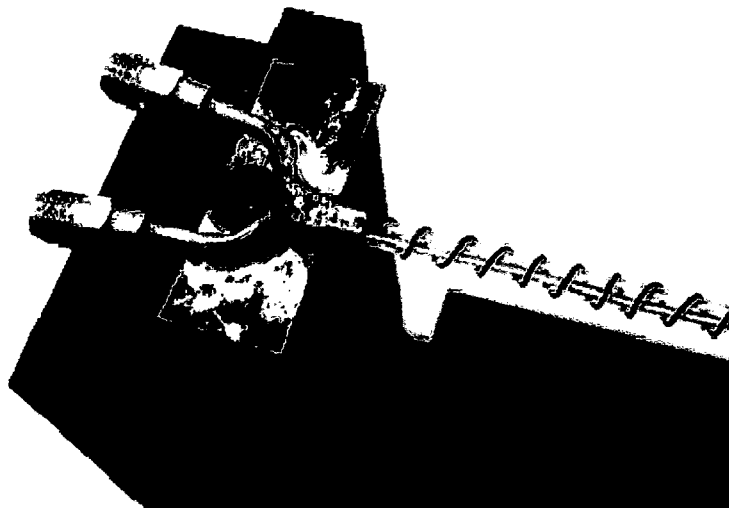


Figure 19: Shield Connection with Solder

Experiment One is an unshielded differential transmission, which provides the baseline for the DUT. Experiment Two is of a longitudinally-wrapped copper foil shield. Experiments Three through Ten are composed of a series of differential transmission measurements where shielding applied to the DUT is spirally wrapped 30 AWG (0.010 inches diameter) wire with 0.00475 inches of insulation. The width of the wire remains constant for this round of measurements while the longitudinal distance between each winding (turn spacing) varies from 0.160 inches, 0.200 inches, 0.400 inches, 0.530 inches, 0.590 inches, 0.649 inches, 0.850 inches, and 1.200 inches. Consequently, varying this distance proportionately varies the overall length of the shield and the angle of the shield with respect to the signal conductors.

A representative isometric view of the DUT with 30 AWG wrapped wire is displayed in Figure 20. The turn spacing (t) is defined as the length \overline{AB} .

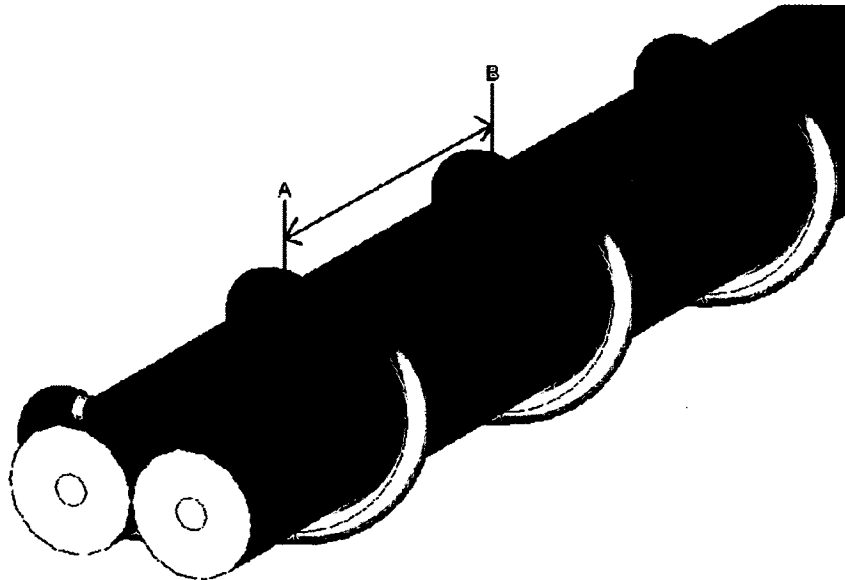


Figure 20: Isometric View of 30 AWG Wire Applied as the Shield to the DUT

One mil (0.001 inch) thick copper foil is spirally wrapped for the shielding in experiments Eleven through Thirteen. Experiments Eleven and Twelve use a shield width (*Width A* in Figure 21) of 0.200 inches and the turn spacing in the winding of the shield is varied from 0.480 inches to 0.850 inches. Experiment Thirteen uses a shield width (*Width A*) of 0.100 inches with a turn spacing of 0.850 inches. The DUT in experiments Fourteen through Twenty-One is spirally wrapped in aluminized polyester shielding. The width (*Width A*) of this shield is 0.200 inches while the turn spacings are 0.160 inches, 0.200 inches, 0.400 inches, 0.530 inches, 0.590 inches, 0.649 inches, 0.850 inches, and 1.200 inches. The experiment with a turn spacing of 0.160 inches has an overlap in the spiral shield. A representative isometric view of the experiments with foil wrapping applied as the shield is illustrated in Figure 21. The turn spacing (t) is defined as the length \overline{AB} . *Width A* is the width of the shield wrap perpendicular to the longitudinal axis if it were unwrapped and straightened, while *Width B* is the width of the shield wrap along the longitudinal axis while it is applied to the DUT.

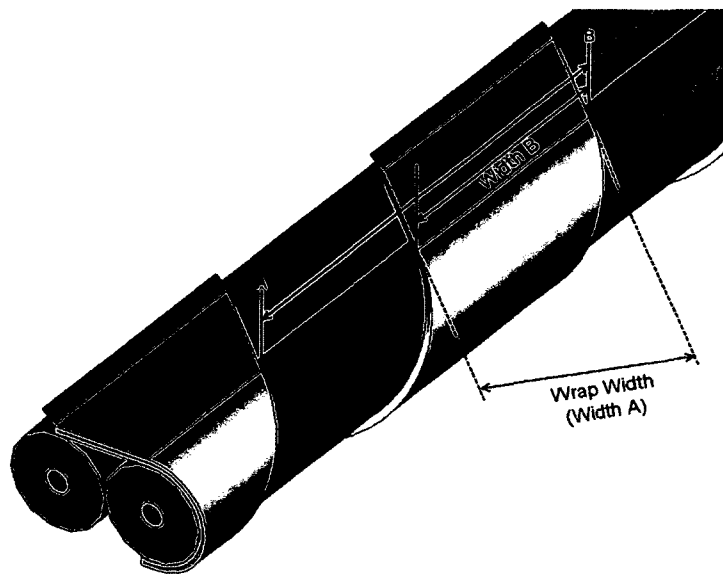


Figure 21: DUT With Spirally Wrapped Foil Applied as the Shielding Structure

Table 1 displays the DUT configurations for this series of measurements.

Experiment	Figure Number	Shield Material	Width A	Turn Spacing
1	Figure 23	None	N/A	N/A
2	Figure 23	Copper Foil	N/A	N/A
3	Figure 24	30 AWG Wire	0.010in.	1.200in
4	Figure 24, Figure 26	30 AWG Wire	0.010in.	0.850in.
5	Figure 25	30 AWG Wire	0.010in.	0.649in.
6	Figure 24, Figure 25	30 AWG Wire	0.010in.	0.590in
7	Figure 25	30 AWG Wire	0.010in.	0.530in.
8	Figure 24	30 AWG Wire	0.010in.	0.400in.
9	Figure 24	30 AWG Wire	0.010in.	0.200in.
10	Figure 24	30 AWG Wire	0.010in.	0.160in..
11	Figure 26, Figure 27, Figure 28	Copper Foil	0.200in.	0.850in.
12	Figure 28	Copper Foil	0.200in.	0.480in.
13	Figure 26	Copper Foil	0.100in.	0.850in.
14	Figure 29	Aluminized Polyester Foil	0.200in.	0.1200in.
15	Figure 27, Figure 29	Aluminized Polyester Foil	0.200in.	0.850in.
16	Figure 29	Aluminized Polyester Foil	0.200in.	0.649in.
17	Figure 29	Aluminized Polyester Foil	0.200in.	0.590in.
18	Figure 29	Aluminized Polyester Foil	0.200in.	0.530in.
19	Figure 29	Aluminized Polyester Foil	0.200in.	0.400in.
20	Figure 29	Aluminized Polyester Foil	0.200in.	0.200in.
21	Figure 29	Aluminized Polyester Foil	0.200in.	0.160in.

Table 1: Experimental DUT shield configurations, 30 AWG

The center frequency of the resonance in the transmission measurements was determined using the following method. First, differential transmissions are plotted with a linear regression line calculated from the transmission data in the range of frequency from 10MHz to a frequency slightly lower than the resonance's low frequency. The bandwidth and the cutoff frequency are calculated from the "3dB" crossing points. 3dB was subtracted from the calculated linear regression line and used as the "3dB" limit line.

“3dB” frequency values of the differential transmissions are taken from points where transmission data crosses the “3dB” limit line. The lower crossing frequency (f_{low}) is the “3dB” low point while the higher crossing frequency (f_{high}) is the “3dB” high point. The resonant frequency is defined in Equation 2.

$$\left[f_{low} + \frac{(f_{high} - f_{low})}{2} \right] \quad [2]$$

A representative plot displayed in Figure 22. When this method cannot be used because of measurement frequency limitations, the frequency of largest attenuation is chosen as the center frequency of the resonance.

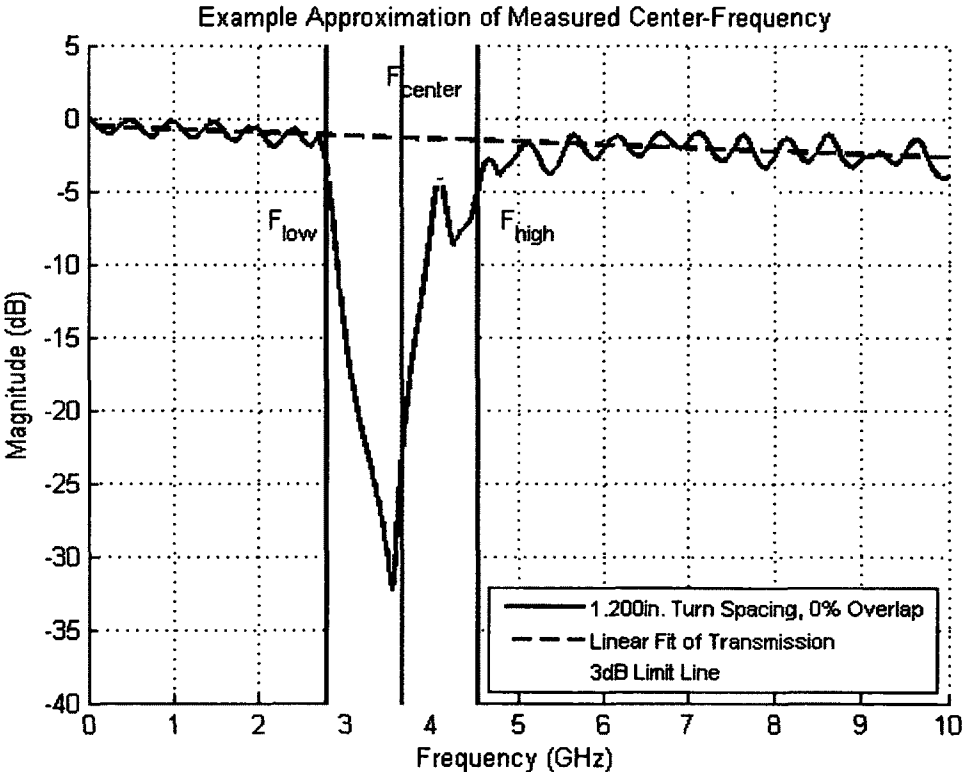


Figure 22: Center frequency calculation of the resonant behavior in a transmission

Figure 23 illustrates the differential transmissions (S_{DD21}) through the DUT with no shielding and with a longitudinally wrapped copper foil shield. Transmission of the DUT with no shielding experiences 2.5 dB of variation due to significant impedance mismatch between the measurement environment and the transmission line. This variation increases slightly with frequency. When shielded with a longitudinally wrapped copper foil shield, the transmission line exhibits a minimal combing due to impedance mismatching from 0GHz to 4GHz. In the range of 4GHz to 20GHz, this shielded transmission line configuration experiences slight variation due to impedance mismatch.

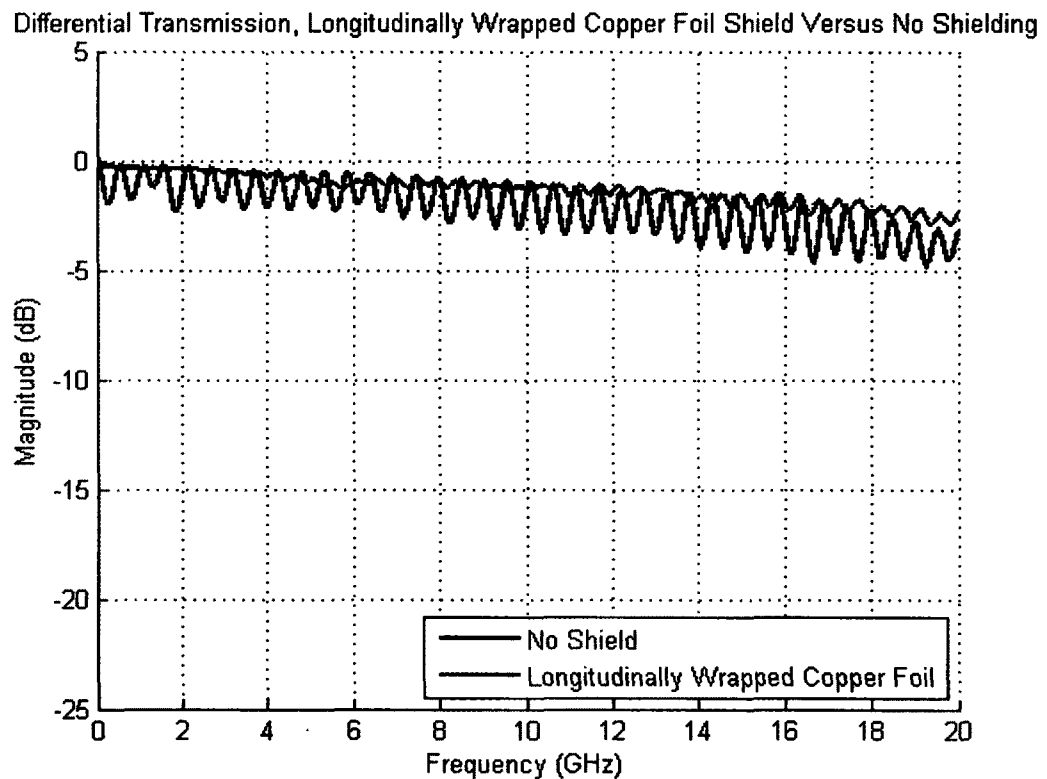


Figure 23: S_{DD21} , DUT , No Shielding vs. Longitudinally Wrapped Copper Foil Shield

Figure 24 illustrates the differential transmissions (S_{DD21}) of the DUT transmission line with 30 AWG insulated wire spirally applied as the shielding structure as a function of turn spacings.

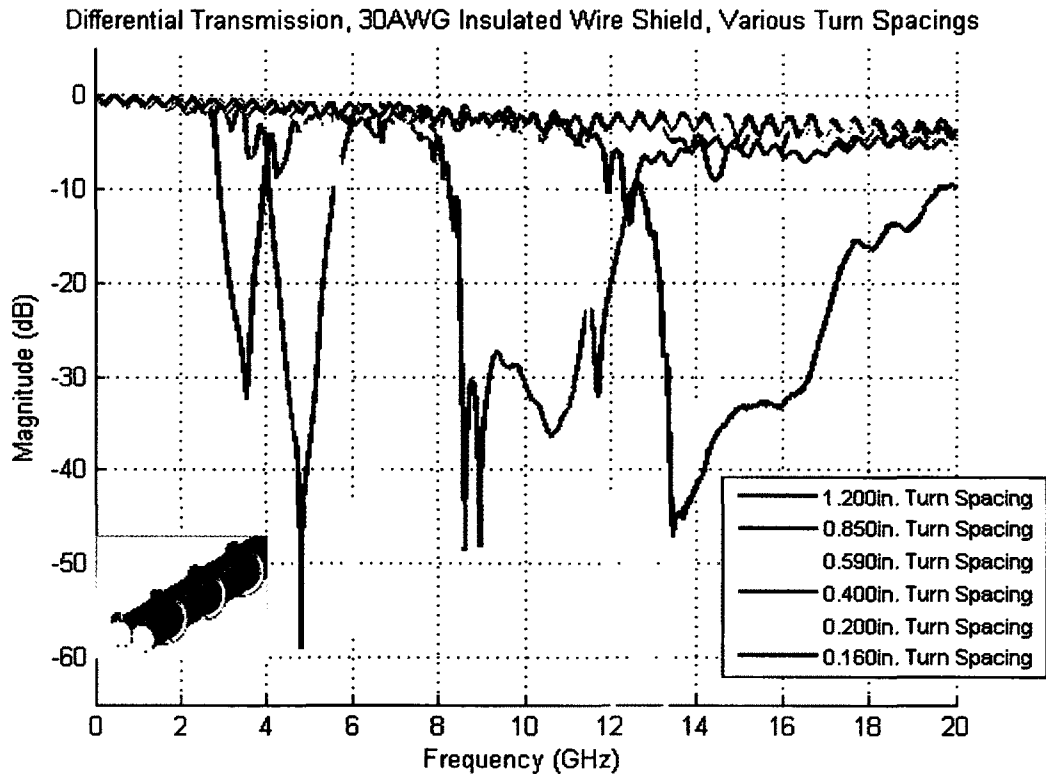


Figure 24: S_{DD21} , DUT, Spiral 30 AWG Shields

Resonant behavior in the transmission when the spiral shield's turn spacing is 1.200 inches occurs with the center frequency at 3.54GHz. A turn spacing of 0.850 inches causes resonant behavior with the center frequency at 4.80GHz. Resonant behavior centered at 6.78GHz when the DUT had shielding applied with a turn spacing of 0.590 inches. A turn spacing of 0.400 inches causes the transmission line to exhibit resonant behavior with a center frequency of 8.60GHz. A turn spacing of 0.200 inches in the shield produced a resonance with the center at 11.74GHz. Transmission through the

DUT with a spiral shield applied with a turn spacing of 0.160 inches experiences resonant behavior at the approximated center frequency of 13.46GHz.

Figure 18 illustrates the differential transmission through the 30 AWG (with 0.00475 inch insulation) spirally wrapped DUT with three different turn spacings. The median turn spacing value of 0.590 inches serves as a baseline, while the 0.530 inches and 0.649 inches turn spacing values serve as ten percent short and longer turn spacing respectively. This study was performed to validate the robustness of the experimental structure when the turn spacing was varied slightly.

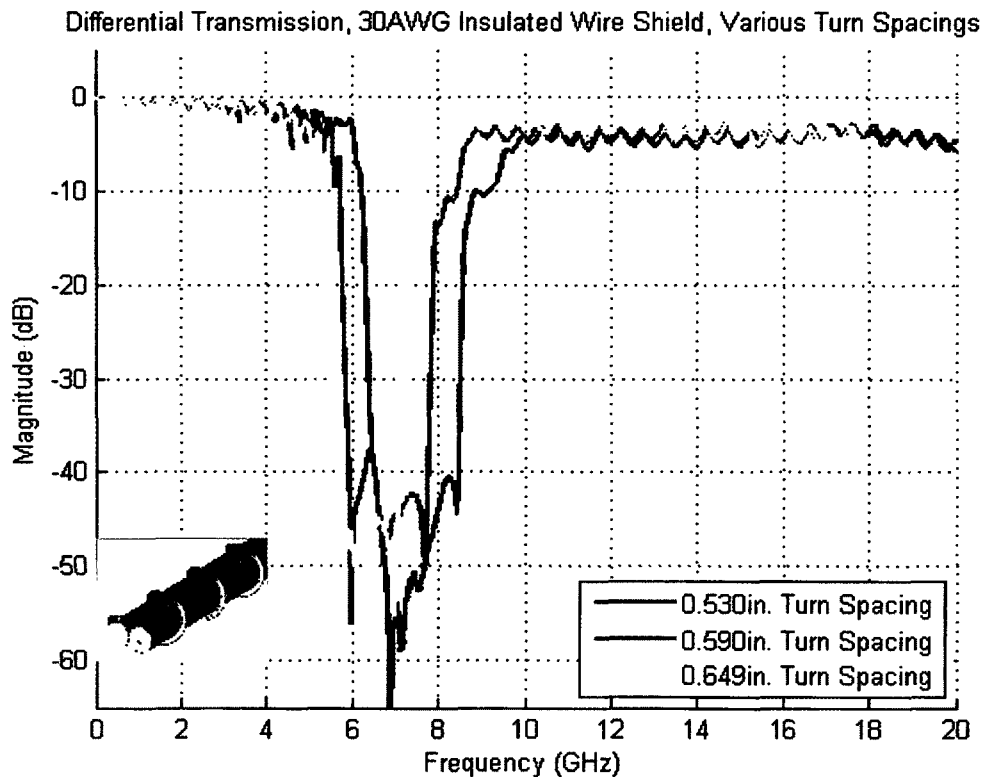


Figure 25: S_{DD21} , DUT, Spiral 30 AWG shields, 10% Turn Spacing Variance

Figure 26 displays the differential transmission exhibited by the DUT with three wrap geometries and constant turn spacing of 0.850 inches. For 0.200 inch wide copper foil shielding, the resonant center frequency is 5.17GHz. This transmission line configuration also experiences a resonance at the second harmonic. Application of 0.100 inch wide copper foil shielding causes the transmission to experience resonant behavior at 5.50GHz. This shield configuration also induces a second harmonic resonance. Transmission through the DUT with spirally wrapped 0.010 inch wire applied as the shield structure experiences resonant behavior at 4.80GHz. This transmission also experiences resonant behavior at the third harmonic of the primary resonant frequency.

Differential Transmission, Spirally Wrapped Shield, 0.850in. Turn Spacing, Various Wrap Widths

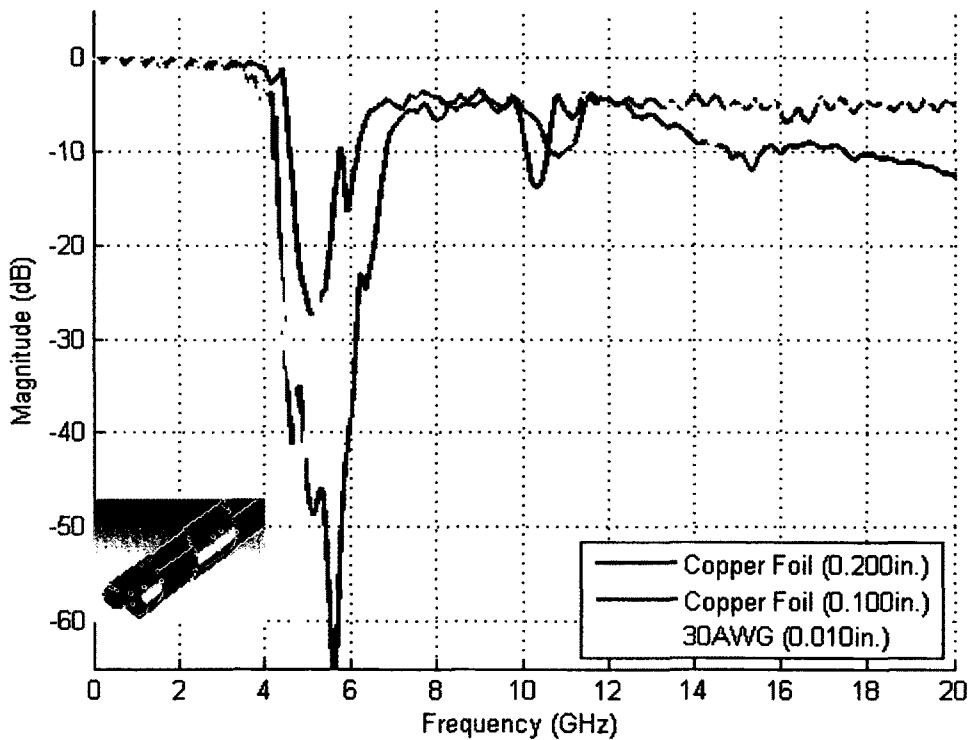


Figure 26: S_{DD21}, DUT, Varying Spiral Shield Geometry

Figure 27 illustrates a study of shield material effect on the differential transmission of the DUT. 0.001 inch thick copper foil and 0.001 inch thick aluminized polyester are employed as the spirally wrapped shield for the DUT with widths (*Width A*) of 0.200 inches. The turn spacing is held constant at 0.850 inches for both iterations of the experiment. For the copper foil shield the first major resonance occurs at 5.17GHz. Shielding the DUT with the aluminized polyester material caused a similar loss in transmission. The center frequency is 4.92GHz.

Differential Transmission, Spirally Wrapped Shield, 0.850in. Turn Spacing, Various Materials

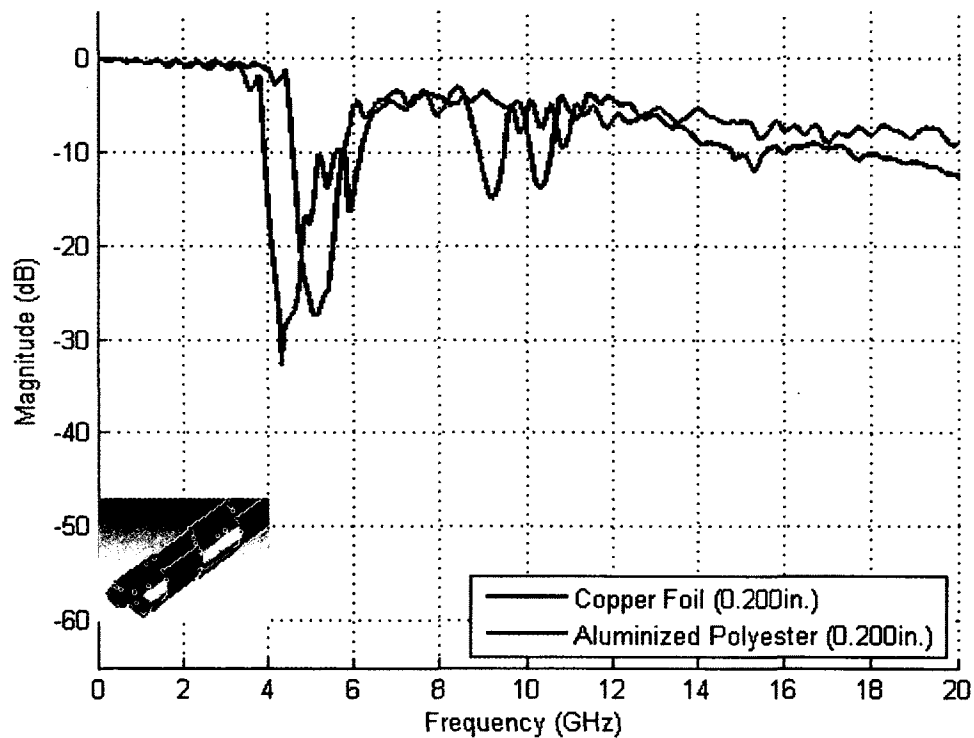


Figure 27: S_{DD21} , DUT, Varying Shield Material

Figure 28 illustrates the differential transmissions of the DUT with two spirally wrapped 0.200 inch wide (*Width A*) copper foil shields. The first copper foil shield was applied with a turn spacing of 0.850 inches, while the second was applied with a 0.480 inch turn spacing. A shield with a turn spacing of 0.850 inches causes the differential transmission through the DUT to exhibit a notch at the center frequency of 5.17GHz. Differential transmission through the DUT when the spirally wrapped copper shield has a turn spacing of 0.480 inches experiences a notch centered at 8.01 GHz.

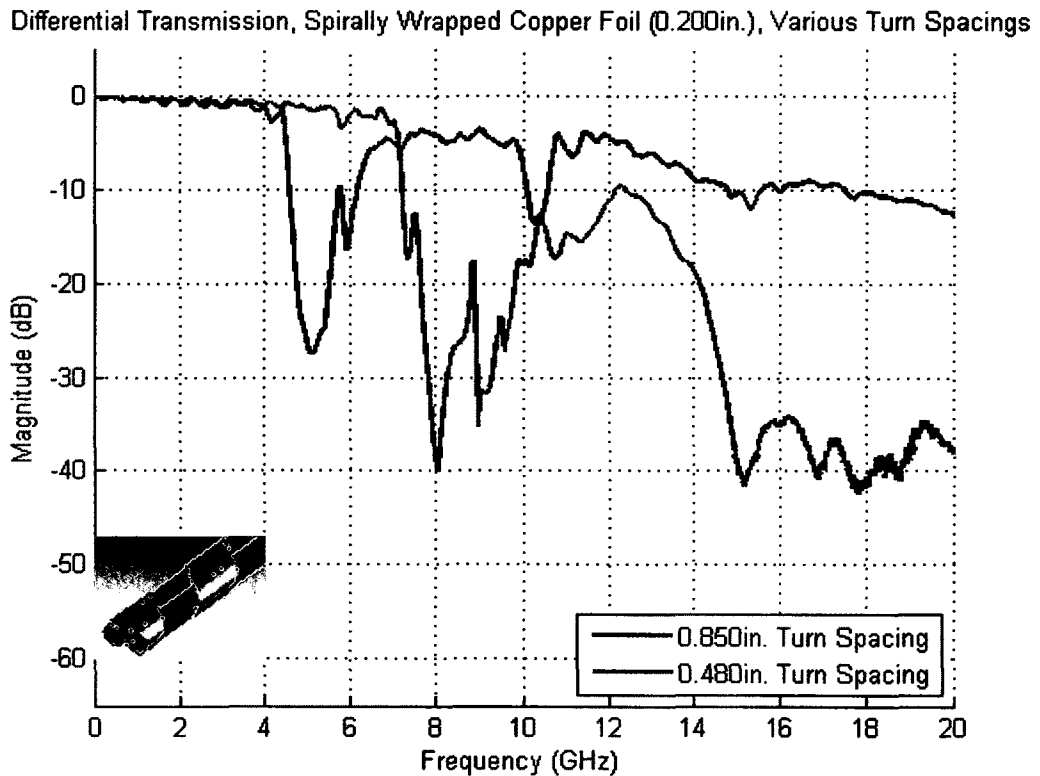


Figure 28: S_{DD21} , DUT, Spiral Copper Foil Shields

Figure 29 displays the differential transmission through the DUT with six different turn spacings and a constant shield *Width A* of 0.200 inches, and a constant material of aluminized polyester foil.

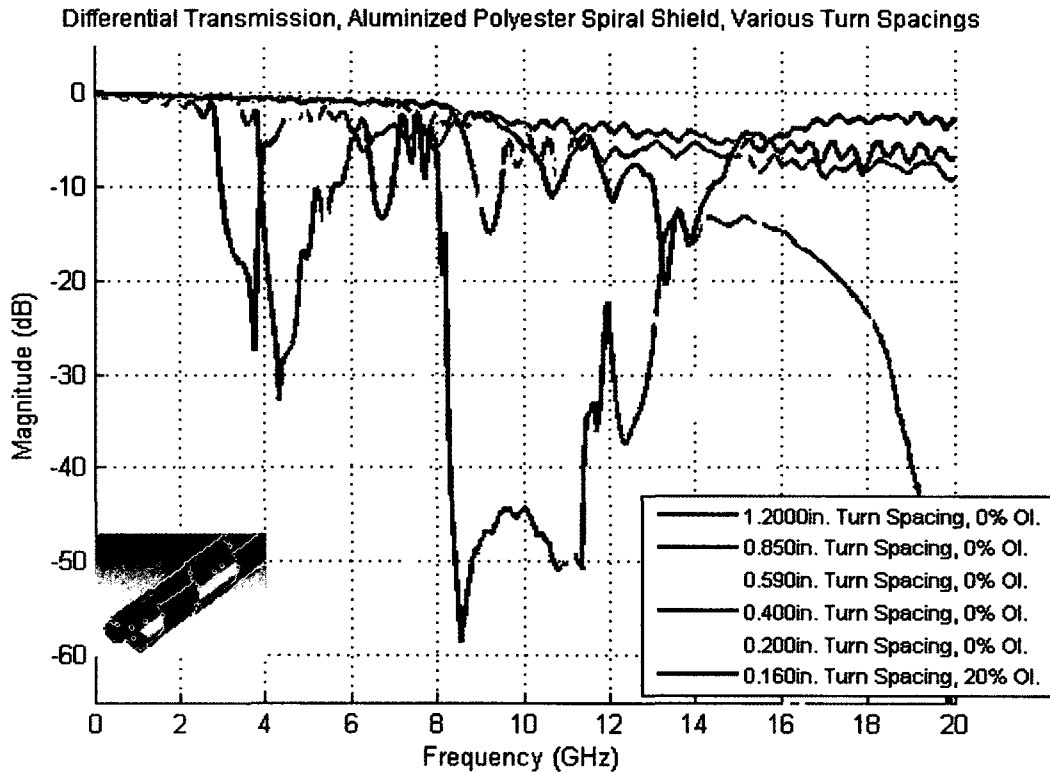


Figure 29: SDD₂₁, DUT, Spiral Aluminized Polyester Shields

This series of six measurements examines the effect of overlap on transmission and center frequency approximation. When the DUT is spirally shielded with a turn spacing of 1.200 inches, the center frequency of the resonance is 3.76GHz. Transmission with a turn spacing of 0.850 inches experiences resonant behavior centered at 4.84GHz. Transmission with a turn spacing of 0.590 inches experiences resonant behavior that is centered at 6.78GHz. With a turn spacing of 0.400 inches, transmission exhibits resonant behavior centered at 8.56GHz. When the turn spacing is 0.200, the spiral shield has near-

zero gap between turns. For this case, the center frequency of the resonance is 11.02GHz. When the shield has an overlap of 20%, the turn spacing is 0.160 inches. For this case, the notch has less attenuation than other cases, and has a center frequency of 13.30GHz. This shield geometry also follows the trend of increasing resonant frequency as the turn spacing decreases.

Figure 30 illustrates the differential transmission through the aluminized polyester foil-wrapped DUT with three different turn spacings. The median turn spacing value of 0.590 inches serves as the baseline, while the 0.530 inch and 0.649 inch turn spacing values serve as ten percent shorter and longer respectively.

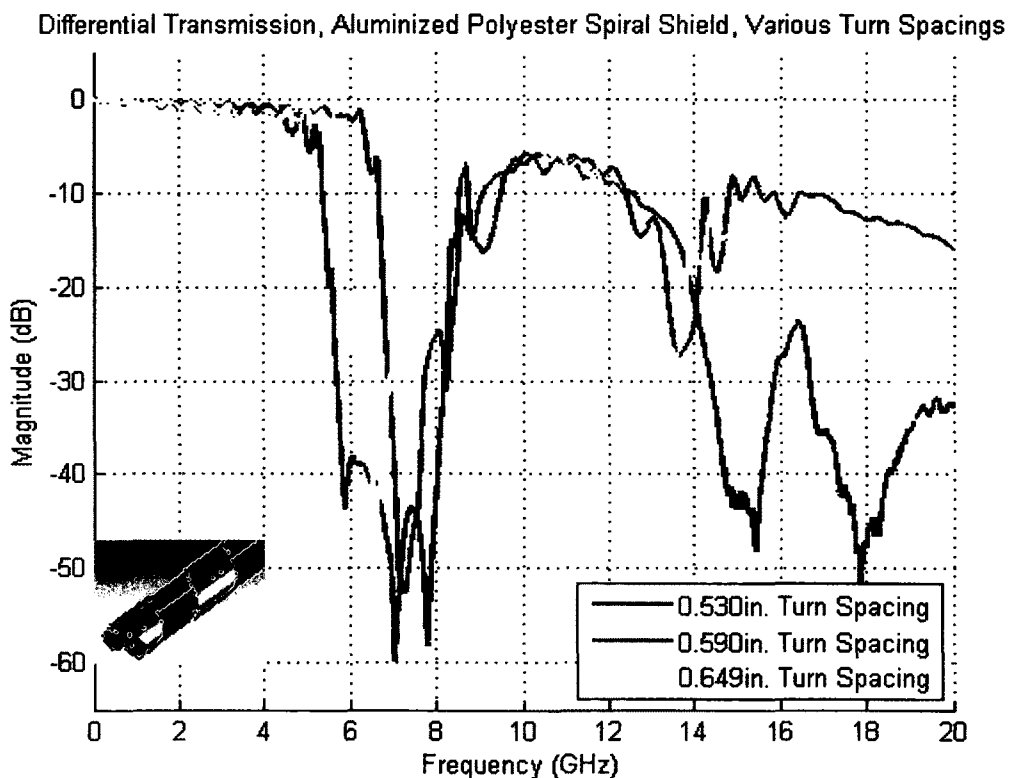


Figure 30: S_{DD21} , DUT, Spiral Aluminized Polyester Shields, 10% Turn Spacing Variance

3.3 Results

From Ramo and Whinnery [Ram53], the propagation constant is found by

$\gamma = \alpha + j\beta = \sqrt{(R + j\omega L)(G + j\omega C)}$, where γ is the complex propagation constant, α is the attenuation constant, and R , L , G , and C are the transmission line characteristics per meter based on the circuit model provided in Figure 31.

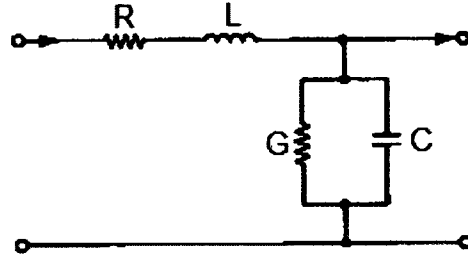


Figure 31: Transmission Line Circuit Model

Because the frequency range that the DUT was measured in is considered high frequency, the loss terms (R and G) may be neglected because $\omega L \gg R$ and $\omega C \gg G$ [And85]. The propagation constant is approximately $\gamma = j\omega\beta$, where $\beta = \omega\sqrt{LC}$. Ramo and Whinnery show that the phase velocity V_p is ω / β , and since $\beta = \omega\sqrt{LC}$, the phase velocity can be approximated by $V_p = 1/\sqrt{LC}$.

To approximate the propagation constant through the DUT structures, 2D quasi-static simulation methods were used. This process was required to justify values for V_p in the proposed equation because the dielectric materials present in significant proximity to the transmission line were inhomogeneous. Consider the DUT structure with no shielding applied. When this is the case, the line parameters L and C were calculated (via quasi-static methods) such that the phase velocity was $2.27 \cdot 10^8$ meters per second.

When the shield of the DUT structure was solid, simulation results yielded L and C parameters such that the phase velocity was $2.02 \cdot 10^8$ meters per second. When the shield was replaced by a wire the phase velocity became $2.17 \cdot 10^8$ meters per second. For DUT structures with 30 AWG wire applied as the shield, the phase velocity was calculated to be $2.27 \cdot 10^8$ meters per second. Since copper and aluminized polyester shields cover a significant percentage of the transmission line, the velocity of propagation for foil shields was calculated to be $2.17 \cdot 10^8$ meters per second.

Turn length l is defined as the length of wire in one turn spacing and is calculated thusly: $\sqrt{t^2 + d^2(\pi + 2)^2}$ where d is the diameter of one signal conductor's dielectric and t is the turn spacing of the applied spiral wrap. V_p is equal to the phase velocity in the

transmission line, and is calculated by $V_p = \frac{1}{\sqrt{LC}}$, where L is the characteristic

inductance of the transmission line in henries per meter and C is the characteristic capacitance of the transmission line in farads per meter. Relating l to a theoretical

resonance, f_{res} , yields $f_{res} = \frac{V_p}{2l} = \frac{1}{2l\sqrt{LC}}$ with the units of GHz.

Table 2 compares the measured resonance center frequency with the theoretical resonant frequency (f_{res}) for cases using spiral wire shields of varying turn spacings.

Table 3 does the same for various spacings of 0.200 inch wide (*Width A*) copper foil shields.

Turn Spacing (Inches)	Turn Length (<i>l</i>) (Inches)	Measured Resonance Center Frequency (GHz)	f_{res} (GHz)
1.200	1.246	3.54	3.59
0.850	0.913	4.80	4.90
0.649	0.730	6.30	6.13
0.590	0.678	6.78	6.60
0.530	0.627	7.46	7.15
0.400	0.521	8.60	8.59
0.270	0.430	10.28	10.42
0.200	0.390	11.74	11.49
0.160	0.370	13.46	12.08

Table 2: Measurement Results, DUT, 30 AWG Spiral Shield

Turn Spacing (Inches)	Turn Length (<i>l</i>) (Inches)	Measured Resonance Center Frequency (GHz)	f_{res} (GHz)
0.850	0.913	5.17	4.69
0.480	0.585	8.01	7.33

Table 3: Measurement Results, DUT, 0.200in. Copper Foil Spiral Shield

Table 4 does the same for various wrap widths (*Width A*) but at a constant turn length.

Wrap Width <i>A</i> (Inches)	Shield Material	Turn Length (<i>l</i>) (Inches)	Measured Resonance Center Frequency (GHz)	f_{res} (GHz)
0.100	Copper Foil	0.913	5.50	4.69
0.200	Copper Foil	0.913	5.17	4.69
0.010	30 AWG	0.913	4.80	4.69

Table 4: Measurement Results, Constant Turn Spacing, Varying Spiral Shield Geometry

Table 5 shows the results collected on the DUT with no ground drain wire when the shield material is 0.200 inch wide (*Width A*) aluminized polyester foil. This center frequency is compared to the theoretic f_{res} .

Turn Spacing (Inches)	Turn Length (<i>l</i>) (Inches)	Measured Resonance Center Frequency (GHz)	f_{res} (GHz)
1.200	1.246	3.76	3.44
0.850	0.913	4.84	4.69
0.649	0.730	6.48	5.87
0.590	0.678	6.78	6.32
0.530	0.627	7.14	6.84
0.400	0.521	8.56	8.22
0.270	0.430	10.11	9.97
0.200	0.390	11.06	11.00
0.160	0.370	13.30	11.56

Table 5: Measurement Results, DUT, Aluminized Polyester Spiral Shield

CHAPTER 4: COMPUTER SIMULATION

Chapter 4 describes the simulation techniques utilized in the examination of twinaxial cables. The chapter details the simulation software packages, the solving methods these tools employ, the limitations and assumptions made by these tools and their environments, and the structures simulated in each tool. Full-wave models and equivalent circuit models are evaluated, with circuit model parameters collected via quasi-static simulation methods.

4.1 Full-Wave Simulation Tool

In this study the frequency responses of twinaxial cables were obtained using a commercially available simulation package. Full-wave simulation of models is performed using the finite integration technique (FIT). Shuhmann describes the Finite Integration Technique in the following way “ [finite integration technique] “ is a discretization method which transforms Maxwell’s equations onto a dual grid cell complex, resulting in a set of discrete matrix equations. The degrees of freedom collected in the vectors of this discretization scheme, typically consist in physically measurable, integral quantities such as voltages, currents or charges” [Sch96]. The software package utilizing FIT in the solving routine computes the integral form of Maxwell’s equations for the discretized model. These solutions depict how a structure will respond to a source. The resultant outputs of the simulation software package are the frequency domain scattering parameters along with the time domain impulse response.

4.2 Full-Wave Modeling and Simulation Technique

The discretization of the simulation space including the model is critical when determining the accuracy of the simulation. The discretization of the space is colloquially referred to as the meshing. Inadequate meshing of the space will provide

inaccurate and misleading results. To ensure adequate meshing, the largest mesh element in the full-wave space was set to be no larger than one-tenth of one wavelength of the upper frequency limit of 40 GHz. The simulated model is differentially excited at each termination by a differential waveguide port.

Twinaxial cables are composed of the following major components: two equivalent signal conductors, dielectric material insulating the signal conductors, a shield, and a ground drain wire. To replicate resonant phenomenon the twinaxial cable with a spiral shield, a model was created in the full-wave software package. To compensate for software constraints and limitations of the algorithms used to discretize the space, the twinaxial model was modified. Similar to the experimental cases, the shield was modeled with a gap rather than an overlap in order to simulate the modified line characteristics induced by the spiral.

The total length of the simulated structure was 5.0 inches due to simulation resource constraints. Perfect electric conductor (PEC) signal conductors are 0.020 inches in diameter and have a 0.065 inch center-to-center spacing. Dielectric material encompassing the signal conductors is 0.065 inches in outside diameter. This material has a relative permittivity (ϵ_r) of 2.25 with a loss tangent ($\tan \delta$) of 0.005. This loss tangent was chosen to enforce stability in the structure. The PEC shield structure in each simulated case is composed of two distinct regions. The first is 1.0 inch long solid shielding 0.010 inch thick, at each end of the model. The second is a 0.010 inch thick, four-sided polygonal shape that has been extruded and rotated about the dielectric to form a spiral shield to form a current path from each of the solid shield members, causing the

longitudinal length of the spiral segment to be 3.0 inches Figure 32 illustrates the simulated twinaxial structure.

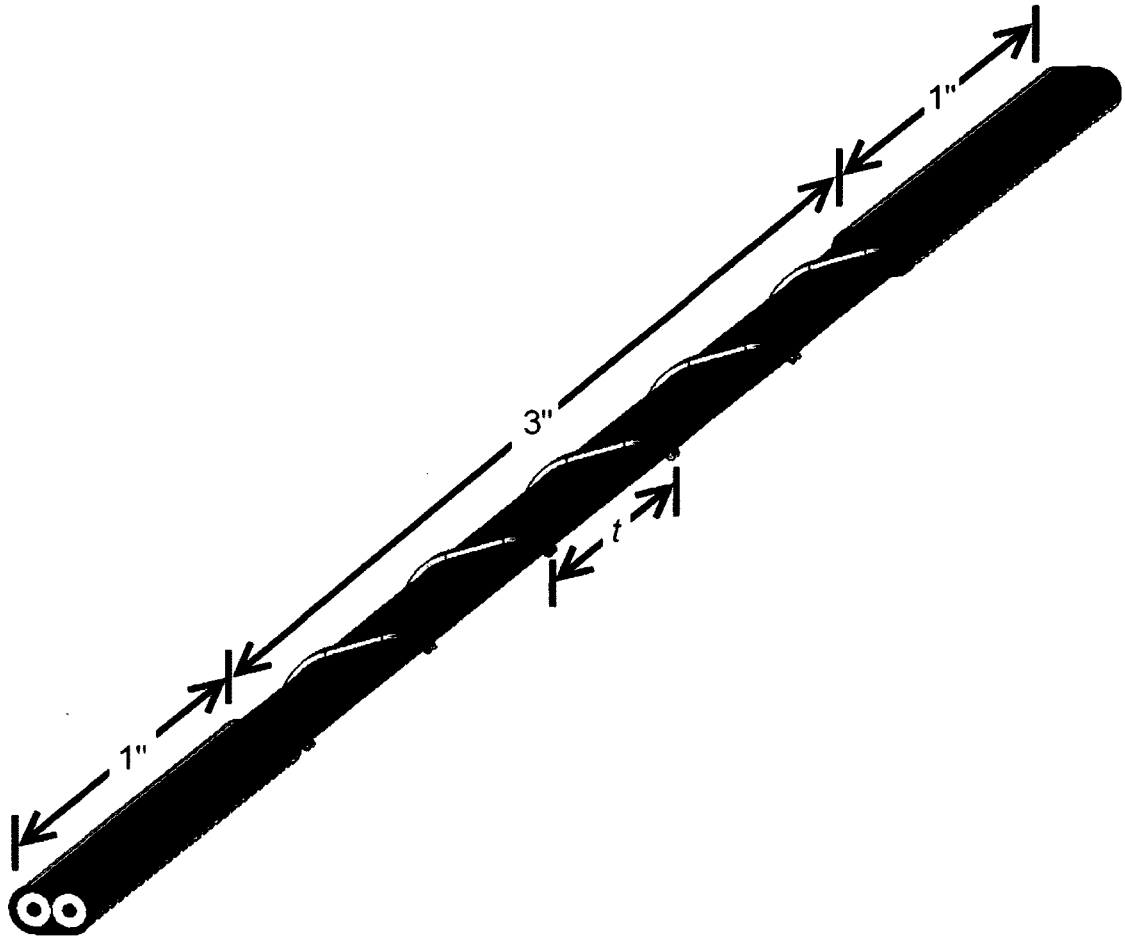


Figure 32: Simulated Twinaxial Structure

Variables in this series of experiments include the turn spacing, t , of the spiral shield structure, and tightness factor of the spiral shield structure. The tightness factor ranges from 0.9 to 1.1 with a default value of 1.0, and describes the result of the tension with which the spiral shield wrap was applied to the pair of insulated wires. The tightness factor was 0.9 for a shield applied with a high tension and 1.1 for a shield applied with a low tension. Values for the tightness factor correspond to the X-Y plane scaling of the spiral shield structure in the simulation environment. In addition to the spiral shield

segments, a completely solid shield case has been simulated to provide a control. Table 6 displays the six simulations performed. The ground drain wire has been neglected for this series of simulations.

Simulation	Figure	Turn Spacing	Tightness Factor
1	Figure 33	n/a, solid shield	1.0
2	Figure 34	0.270in.	1.0
3	Figure 34	0.530in.	1.0
4	Figure 34, Figure 35	0.590in.	1.0
5	Figure 34	0.649in.	1.0
6	Figure 34	1.200in.	1.0
7	Figure 35	0.590in.	0.9
8	Figure 35	0.590in.	1.1

Table 6: Full-wave Simulation Case Details

4.3 Full-Wave Simulation Results

Results for simulation 1 are displayed in Figure 33. The structure simulated is shielded by a solid conductor for the entire length. Losses exhibited by the simulated transmission are induced by dispersion in the dielectric material.

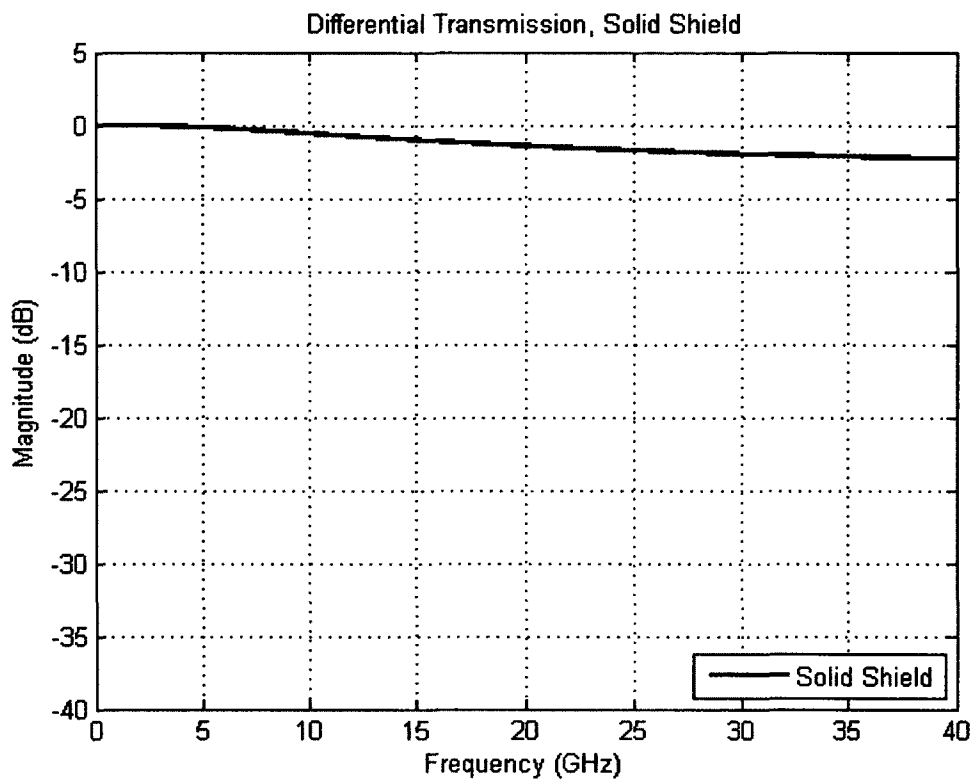


Figure 33: S_{DD21} , Full-Wave Simulation, Solid Shield

Simulated differential transmission for models with spiral shields of the following turn spacing sizes are illustrated in Figure 34: 0.270 inches, 0.530 inches, 0.590 inches, 0.649 inches, and 1.200 inches. Center frequency values are determined via the method highlighted in Figure 22 of Chapter 3, section 2.

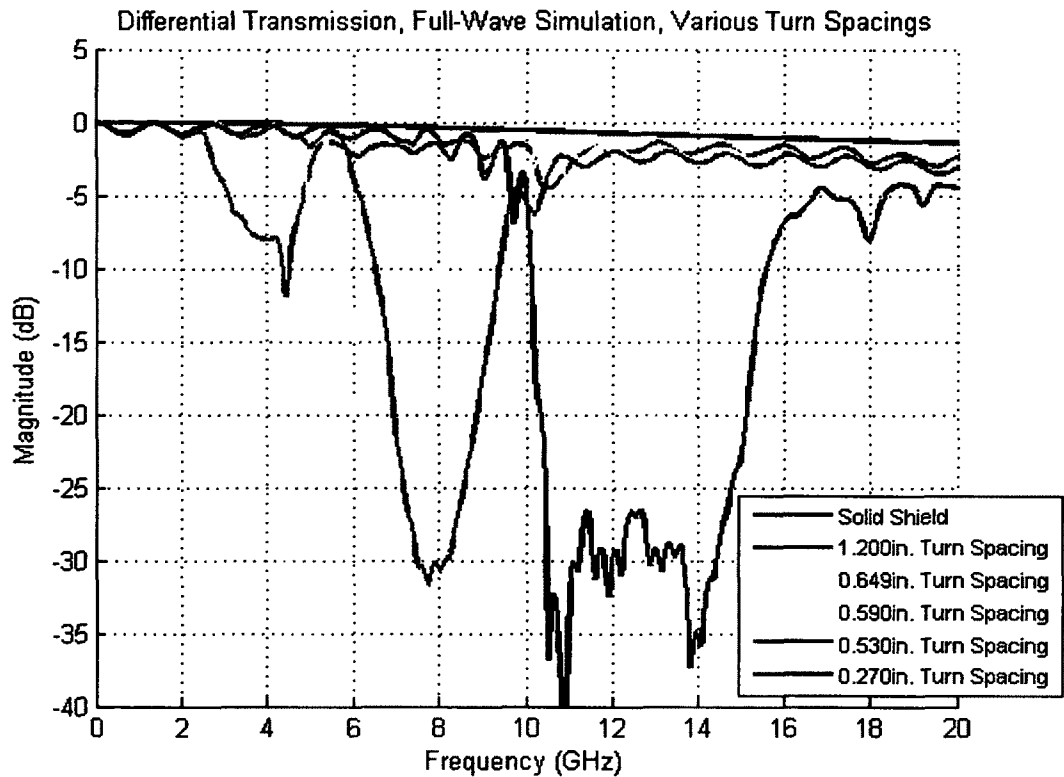


Figure 34: S_{DD21} , Full-Wave Simulation, 30 AWG Spiral Shields

Modeling a spiral shield with a turn spacing of 1.200 inches produced simulated differential transmission with resonant behavior centered at 3.88GHz. A turn spacing of 0.649 inches yields a simulated transmission with a resonance that has a center frequency at 6.44GHz. A turn spacing of 0.590 inches produced a differential transmission with a resonant behavior centered at 6.72GHz. Varying the turn spacing down from 0.590 inches by a factor of 10% to create a spiral with a 0.530 inch turn spacing yields a

differential transmission with a resonant behavior that is centered at 7.76GHz.

Decreasing the turn spacing of the modeled shield to 0.270 inches causes simulated differential transmission to experience a resonance centered at 12.40GHz. Combining in the simulated differential transmissions is due to impedance mismatching in the simulated transmission lines.

Varying the tightness factor of the spiral wrap has an effect that is illustrated in Figure 35. Each simulated differential transmission has a resonance in the range of 5.20GHz to 9.32GHz, with minimal variation in center frequency between cases. As the tightness of the wrap increases, the bandwidth of the notch filter decreases and the maximum attenuation decreases.

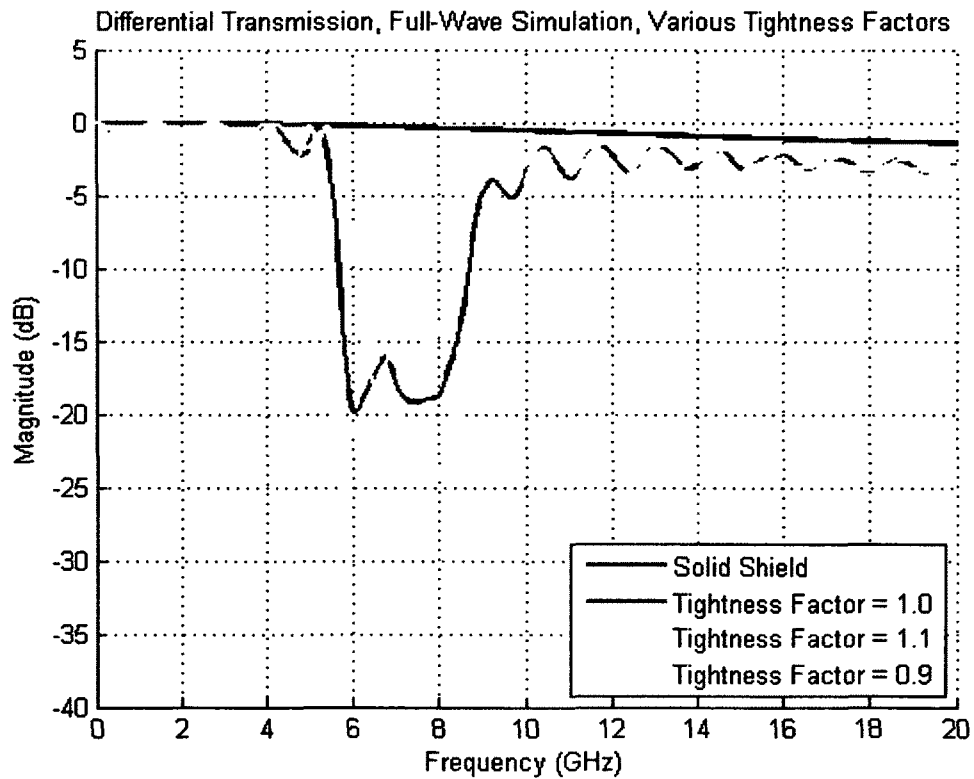


Figure 35, Full-Wave Simulation, Varying Tightness Factor

Full-wave simulation results for varying turn spacings are tabulated in Table 7.

Turn Spacing (Inches)	Turn Length (Inches)	First Resonance Frequency (GHz)	f_{res} (GHz)
1.200	1.246	3.88	3.59
0.649	0.730	6.44	6.13
0.590	0.678	6.72	6.60
0.530	0.627	7.86	7.15
0.270	0.430	12.40	10.42

Table 7: Full-wave Simulation Results, Twinaxial Structures

Full-wave simulation results for varying tightness factors are illustrated in Table

8. The turn spacing of each spiral shield in this set of simulations is 0.590 inches.

Tightness Factor	First Resonance Frequency (GHz)	f_{res} (GHz)
0.9	6.76	6.60
1.0	6.72	6.60
1.1	6.88	6.60

Table 8: Full-wave Simulation Results, Twinaxial Structures, Varying Tightness Factor

4.4 Circuit Model and Analysis Results

A way of thinking about a twinaxial cable structure with a spiral shield is to equate it to a three conductor transmission line. The goal of creating an equivalent circuit model of the twinaxial structure is to predict approximately the first resonance frequency. Although commercial twinaxial cable structures are lossy, to simplify the simulations the losses due to the dielectric and conductor materials are neglected. A common method of describing a lossless transmission line as a lumped element model is the π network (Figure 36).

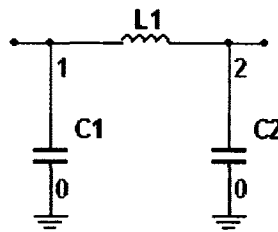


Figure 36: Equivalent Circuit Model of a Two Conductor Lossless Transmission Line

The spiral length of the twinaxial cable is illustrated in Figure 37 will be approximated by four cascaded π networks. When the shield conductor is positioned as in Figure 38, it is more closely coupled to one signal conductor than the other. This will represent the first π network. The complementary shield position (Figure 39) will correspond to the third π network. Figure 40 illustrates the conductor configuration for the π network when the spiral shield conductor is coupled equally to both conductors, and this will represent the second π network and the complementary position (Figure 41) represents the fourth π network.

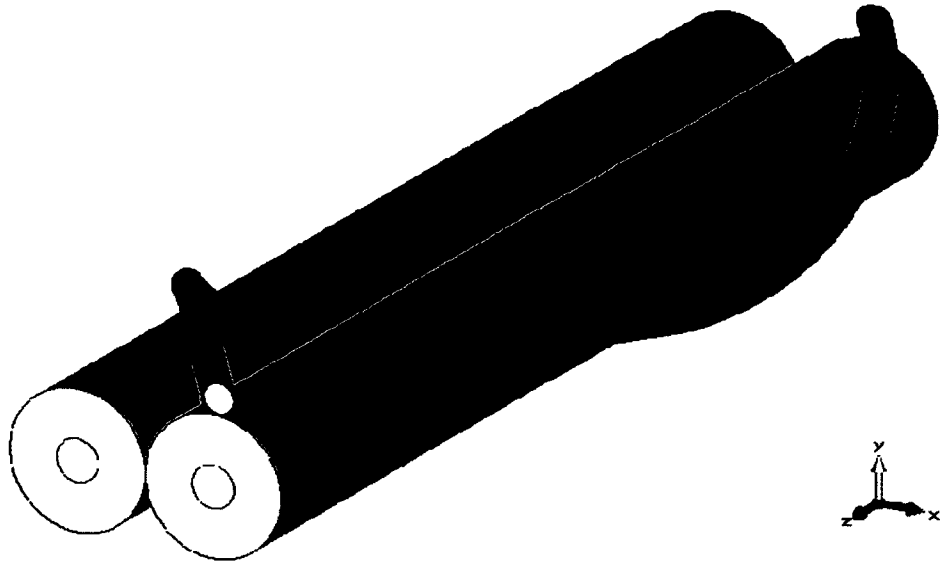


Figure 37: 3D Model of the Twinaxial Transmission Line Structure

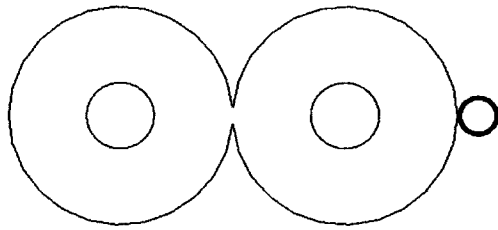


Figure 38: Cross-Section, First π Network Segment

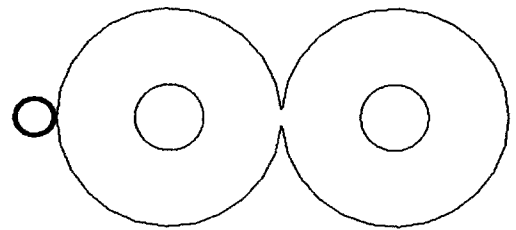


Figure 39: Cross-Section, Third π Network Segment

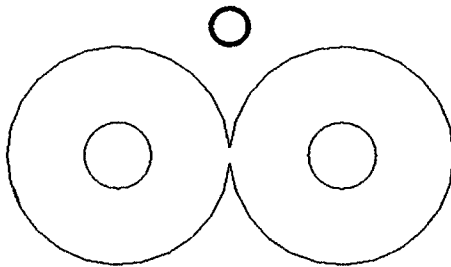


Figure 40: Cross-Section, Second π Network Segment

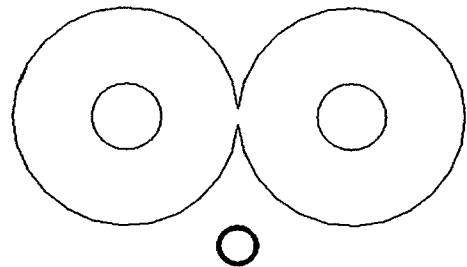


Figure 41: Cross-Section, Fourth π Network Segment

In order to apportion the proper values of inductances and capacitances in each π network, the approximate physical length of each segment is determined by the percentage of the turn spacing of which the π network models represent. For the network with the shield conductor coupling to one signal conductor more than the other the π network physical length is approximately 31% of the turn spacing. For section where the shield conductor is coupling equally to each signal conductor, the physical length of the π network is approximately 19% of the turn spacing (see APPENDIX C). The developed equivalent circuit model for one turn spacing of the modeled twinaxial structure is illustrated in Figure 42. Green highlighted π networks represent sections of the structure where the shield conductor is more greatly coupled to one signal conductor than the other. Yellow highlighted π networks represent sections of the structure where the shield conductor is equally coupled to each signal conductor. Orange highlighted regions accentuate the equivalently modeled spiral shield conductor. Capacitances are derived from the Maxwellian Capacitance Matrix, and the inductances are taken from the computed Partial Inductance Matrix [Nab92].

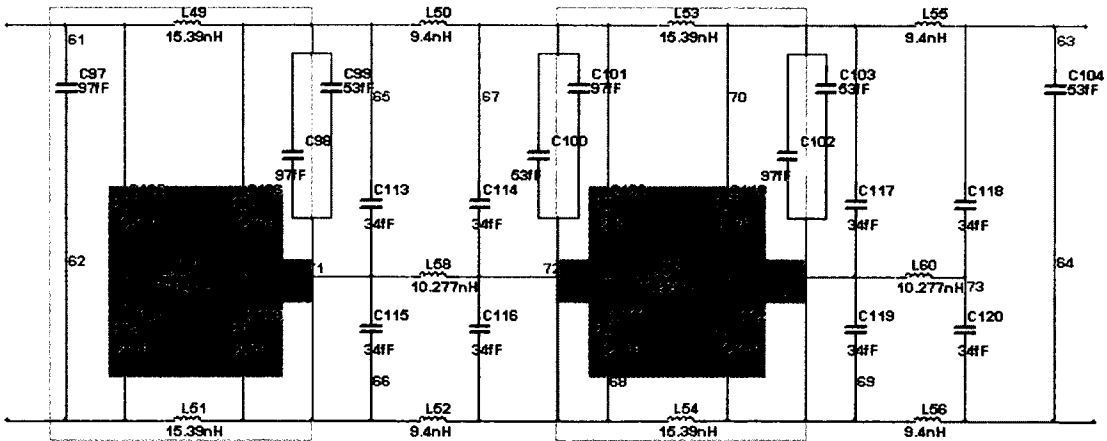


Figure 42: Equivalent Circuit Model for One Turn Spacing of a Twinaxial Structure

Acquisition of transmission line parameters for a twinaxial equivalent circuit model was done via a two-dimensional quasi-static solver. Details on quasi-static solvers are provided in APPENDIX D. Two-dimensional models (illustrated in Figure 38 and Figure 40) for both types of π network segments were created. The dielectric material in these models had a relative dielectric constant of 2.25. Quantities for The Maxwellian Capacitance and Partial Inductance matrices were computed per meter, therefore the values had to be scaled to represent the lengths of each segment of the equivalent circuit model. These matrices computed by the quasi-static solver describe the coupling relationships between the conductors in the model. APPENDIX E provides the actual circuits.

An assumption is made that the equivalent circuit model is valid from 100MHz to the frequency of resonance. π model equivalent circuits are typically valid up to one tenth of one wavelength of the largest physical length represented in the model [Car07].

AC Analysis results for three turn spacing values are illustrated in Figure 43 and summarized in Table 9 with additional results. Evaluation of the proposed equivalent circuit model was done via AC Analysis in SPICE simulations. The AC analysis was performed from 100MHz to 10GHz. The equivalent circuit was differentially excited and the spectrum of the output was computed. Each signal conductor was terminated in the characteristic impedance of the single ended transmission line impedance of 180Ω . The phase velocity was approximated for the model by the method outlined in Chapter 3, and was 2.27×10^8 meters per second. The inductance per unit length was 745nH and the capacitance per unit length was 28.6pF.

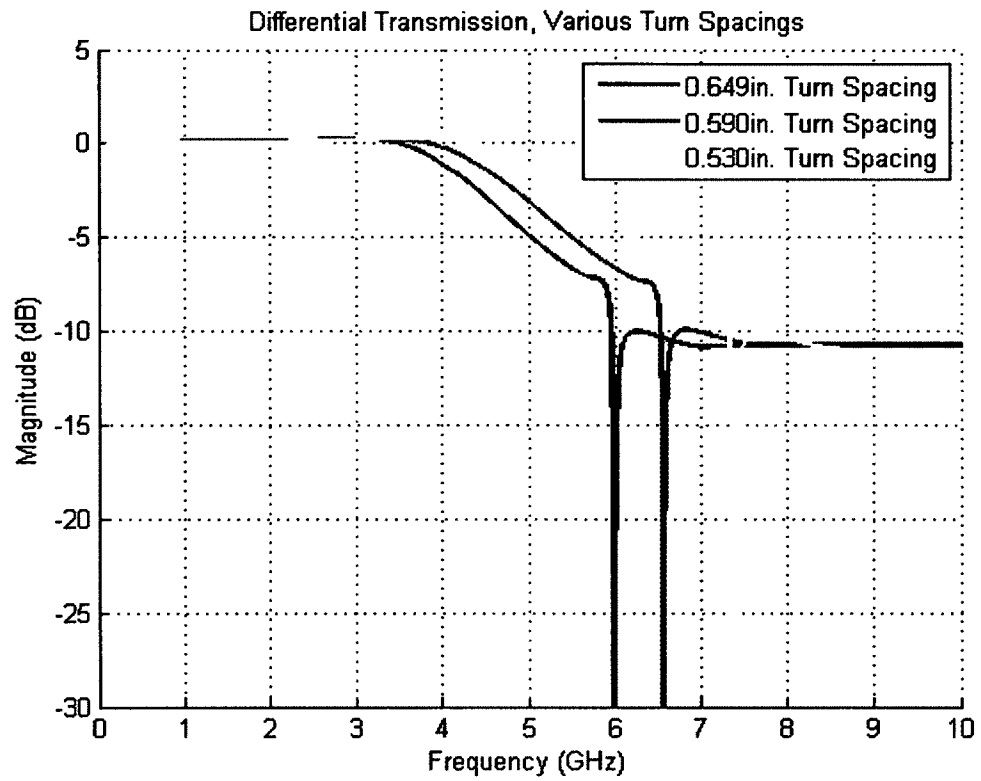


Figure 43: SPICE AC Analysis Results, Equivalent Circuit Models of Twinaxial Structures

Turn Spacing	Turn Length	First Resonant Frequency (GHz)	f_{res} (GHz)
1.200in.	1.246in.	3.22	3.59
0.649in.	0.730in.	5.99	6.13
0.590in.	0.678in.	6.56	6.60
0.530in.	0.627in.	7.34	7.15
0.270in.	0.430in.	13.67	10.42

Table 9: SPICE AC Analysis Results, Equivalent Circuit Models for Twinaxial Structures

CHAPTER 5: Discussion of Results

Chapter V is a comparison of measurements, full-wave simulation models, and the proposed equivalent circuit model. Evaluation of scattering parameter results of experimental and simulated twinaxial structures of various turn spacings is detailed in this chapter. This chapter emphasizes the deficiencies of each simulation methodology and error in measurement. Additionally, comparisons to measured and simulated results of the predictive equation are highlighted.

5.1 Frequency Domain Comparison

Simulation methods and measurement technique are highlighted by the results from this study. Selected frequency domain data from Chapters 3 and 4 are plotted together to offer a comparison between each simulation method and measurement, along with the predicted resonance frequency based upon the turn spacing. The difference in technique is illustrated in Figure 44, Figure 45, Figure 46, Figure 47, and Figure 48. Calibrated measurement data have a higher magnitude of combing than each other set of data due to physical impedance mismatch in the transmission line DUT. Variation between measured center frequencies and predicted center frequencies varied from 50MHz to 310MHz for the selected turn spacings (1.200 inches, 0.649 inches, 0.590 inches, 0.530 inches, and 0.270inches).

From Figure 44 to Figure 48, full-wave simulation results yielded first resonance frequencies 120MHz to 1.98GHz higher than those of the calibrated measurement counterparts. The shape of the resonance and bandwidth of the resonance agree well between the full-wave simulation results and the collected measurements, especially for turn spacings less than 0.270 inches. Since the length of the simulated structure is less than half the length of the measured structure, attenuation is less severe in the resonant region.

The proposed equivalent circuit correlates closely with the predicted center frequency for all turn spacings except for 0.270 inches. In other cases, the range of variation is 40MHz to 370MHz. When the turn spacing of the model was 0.270inches, the predicted center frequency was 3.25GHz lower than the transmission results from the model.

The phase velocity used for calculating f_{res} is common between each data set, and is $2.27 \cdot 10^8$ meters per second.

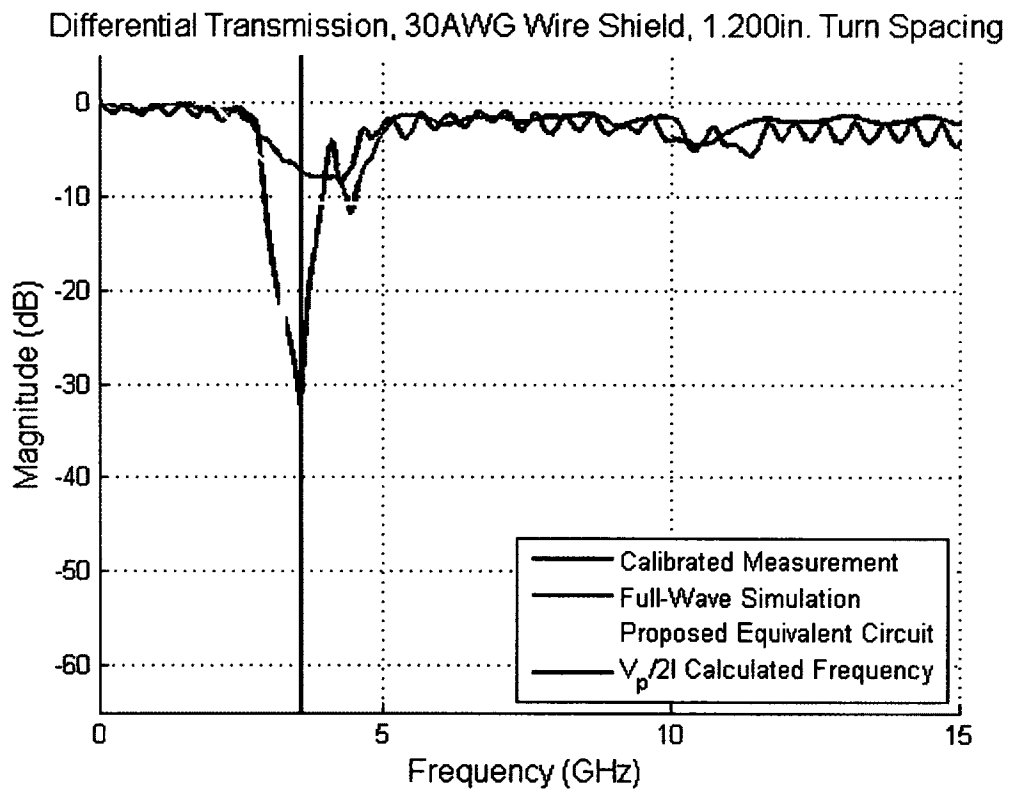


Figure 44: S_{DD21} , Method Comparison, 1.200in. Turn Spacing

Differential Transmission, 30AWG Wire Shield, 0.649in. Turn Spacing

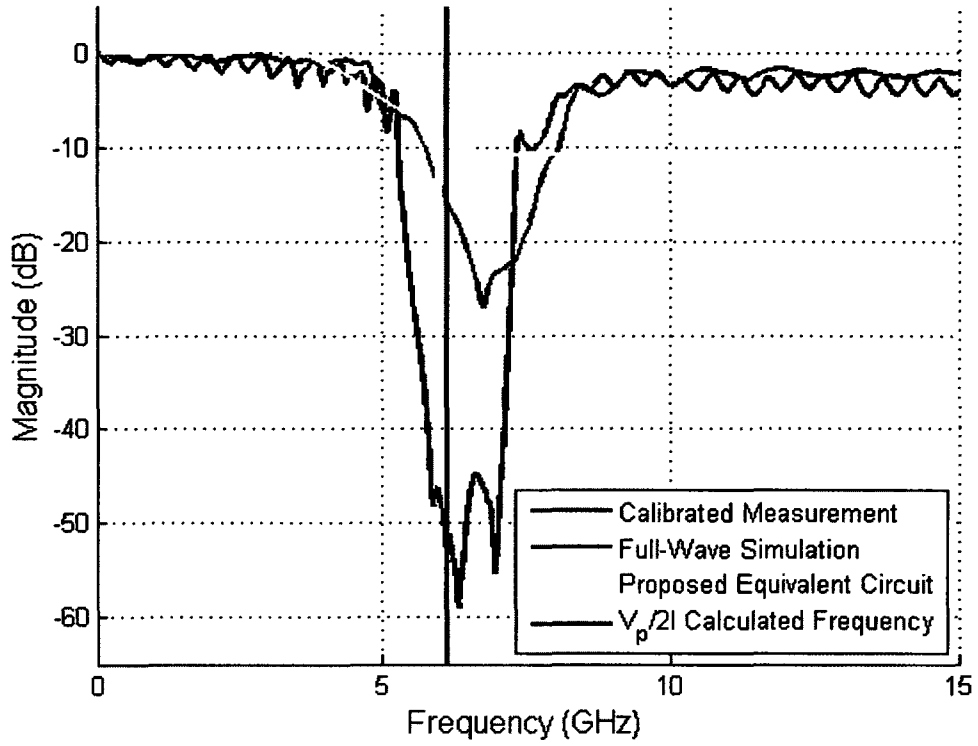


Figure 45: S_{DD21} , Method Comparison, 0.649in. Turn Spacing

Differential Transmission, 30AWG Wire Shield, 0.590in. Turn Spacing

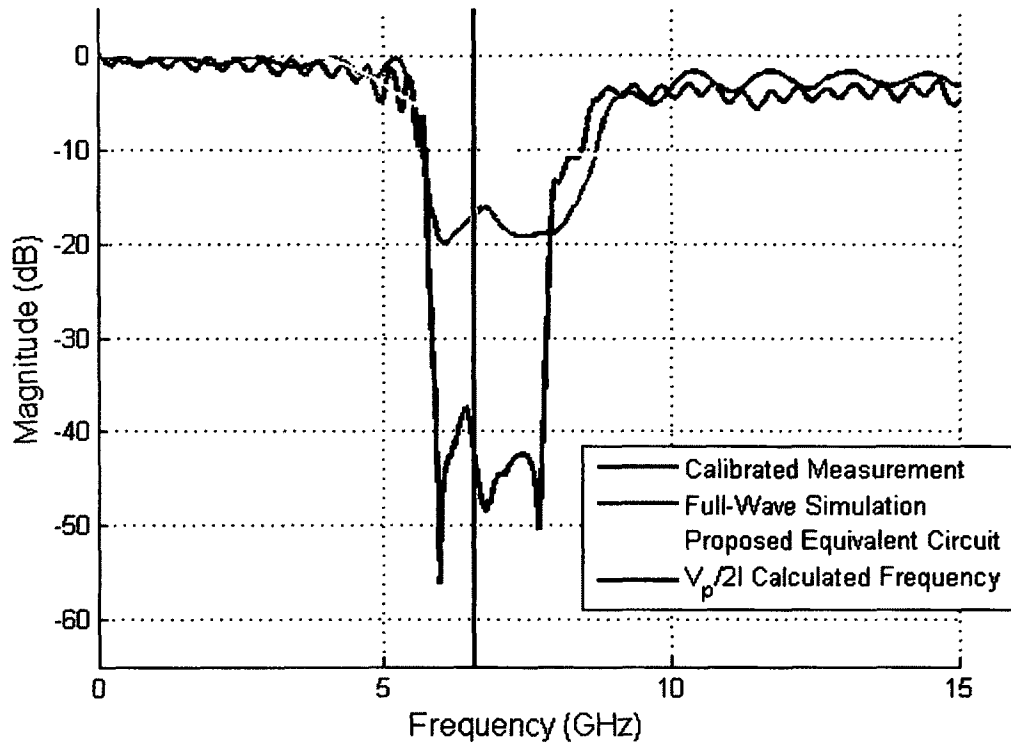


Figure 46: S_{DD21} , Method Comparison, 0.590in. Turn Spacing

Differential Transmission, 30AWG Wire Shield, 0.530in. Turn Spacing

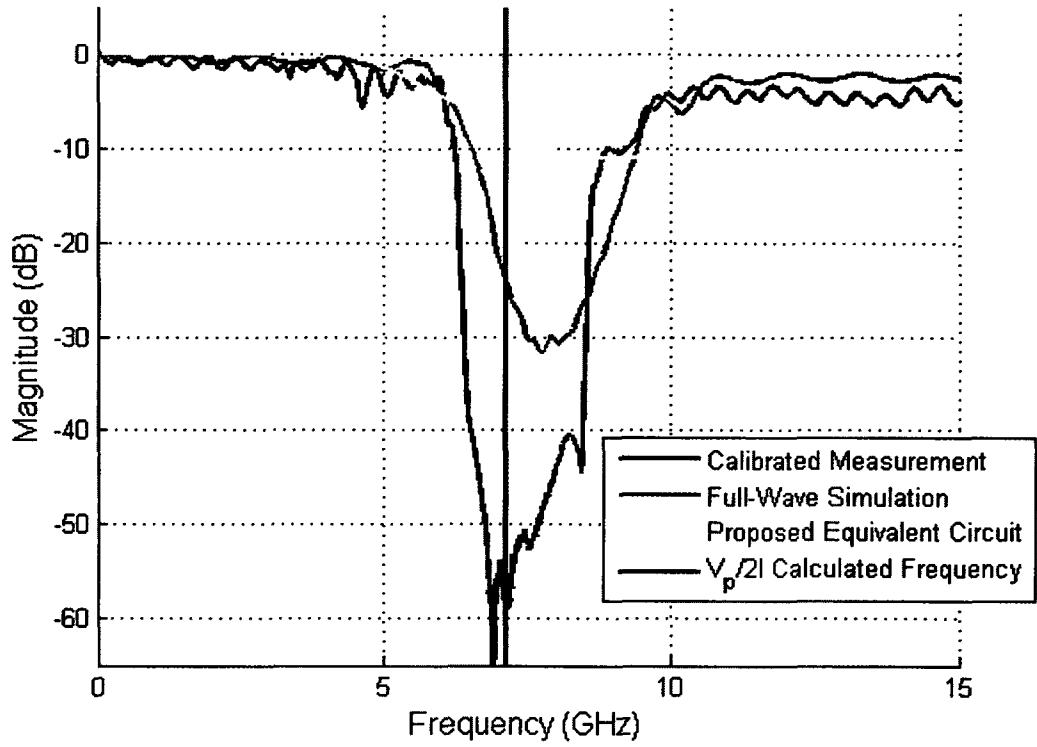


Figure 47: S_{DD21} , Method Comparison, 0.530in. Turn Spacing

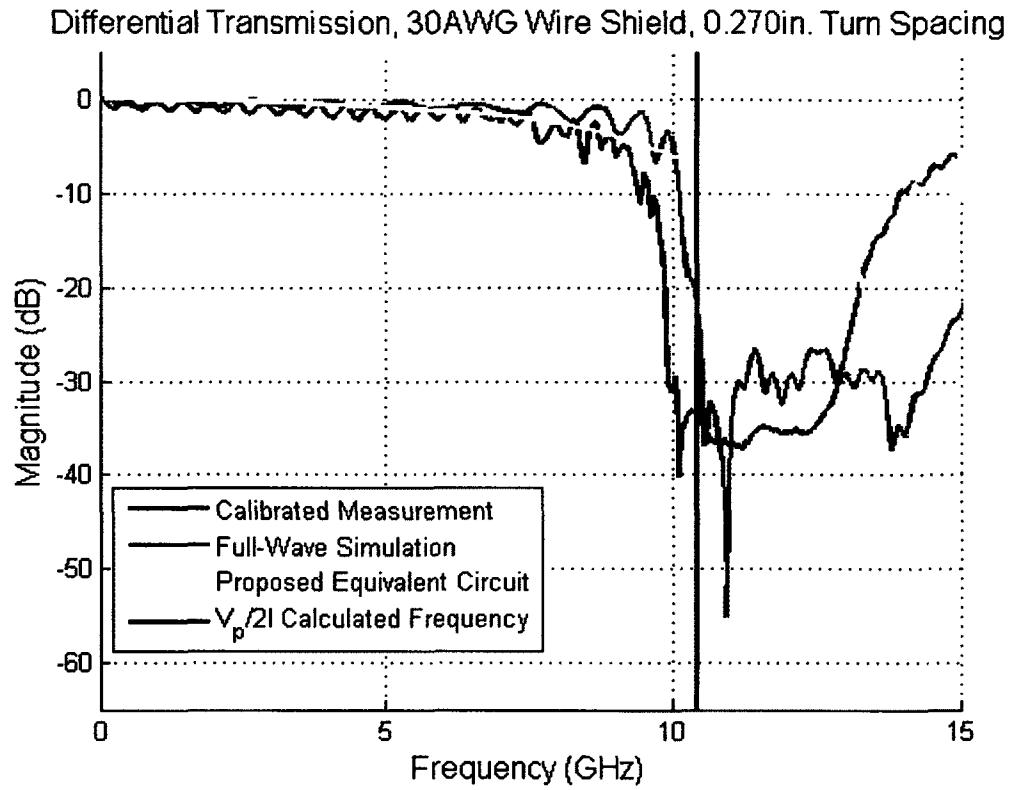


Figure 48: S_{DD21} , Method Comparison, 0.270in. Turn Spacing

Figure 49 displays differential transmission results of one commercial twinaxial cable with a spiral shield and a 0.270 inch turn spacing. Center-frequency agreement exists between the measured set of data and the approximate calculated center frequency by $\frac{1}{2l\sqrt{LC}}$, showing validity of the equation in commercial application. The phase velocity in the commercial cable is 2.30×10^8 meters per second (nominal). This value was taken from the commercial cable's data sheet in Figure B 1, APPENDIX B.

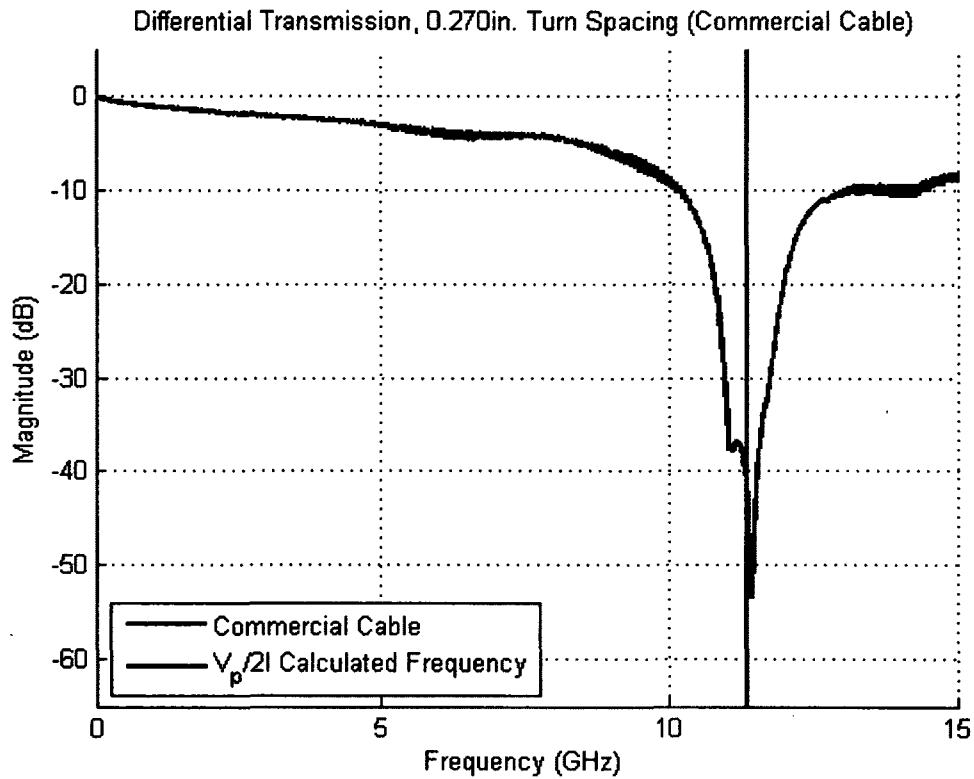


Figure 49: S_{DD21}, Commercial Twinaxial Cable, 0.270in. Turn Spacing

5.2 Summary

The twinaxial structures represented in Figure 50 are the experimental DUT configurations with 30 AWG spiral shields. Overlaid as a scatter plot are the results from measured transmissions of these structures. The predicted resonance center frequency, f_{res} , is calculated for each turn spacing by using Equation 3, where V_p is the phase velocity of the transmission line, d is the outside diameter of the dielectric material encompassing one signal conductor, and t is the turn spacing.

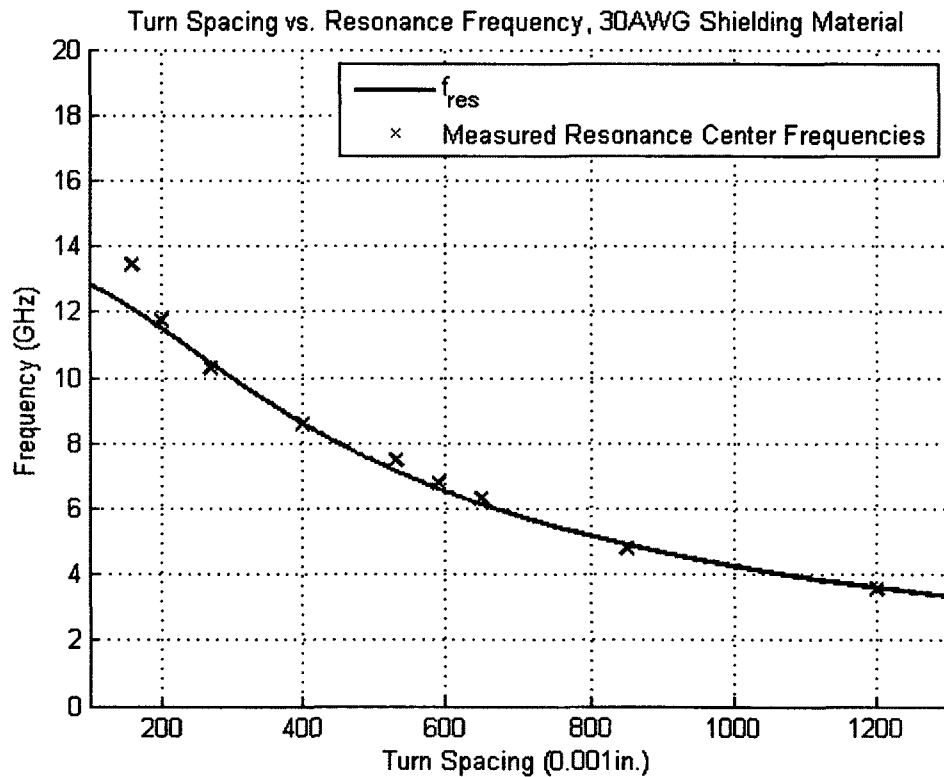


Figure 50: Measured Resonance vs. Predicted Resonance, 30 AWG Spiral Shields

$$f_{res} = \frac{V_p}{2\sqrt{t^2 + d^2(\pi + 2)^2}} \quad [3]$$

Figure 51 compares the center of the resonance frequency in the transmission of a twinaxial structure to the predicted center frequency using the measurement data collected from DUT structures with spirally wrapped aluminized polyester shield. Data from these measured structures is overlaid as a scatter plot.

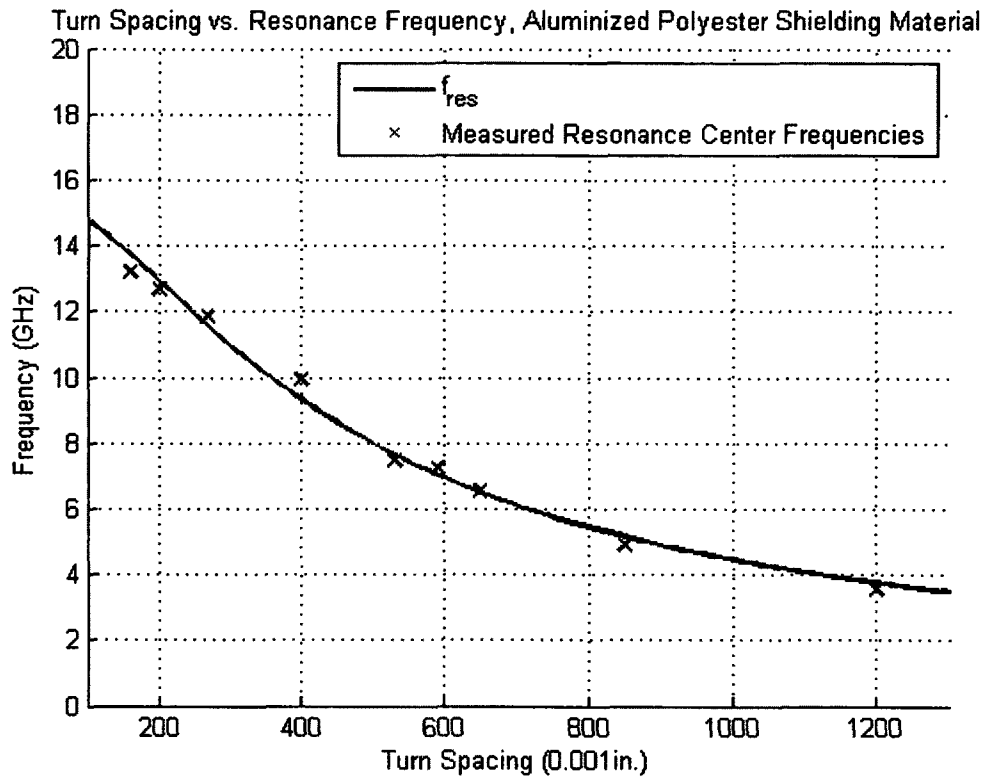


Figure 51: Measured Resonance vs. Predicted Resonance, 0.200in. Wide (*Width A*) Aluminized Polyester Spiral Shields

Figure 52 shows the center frequencies obtained from full-wave simulations of the model compared to predicted resonance center frequencies.

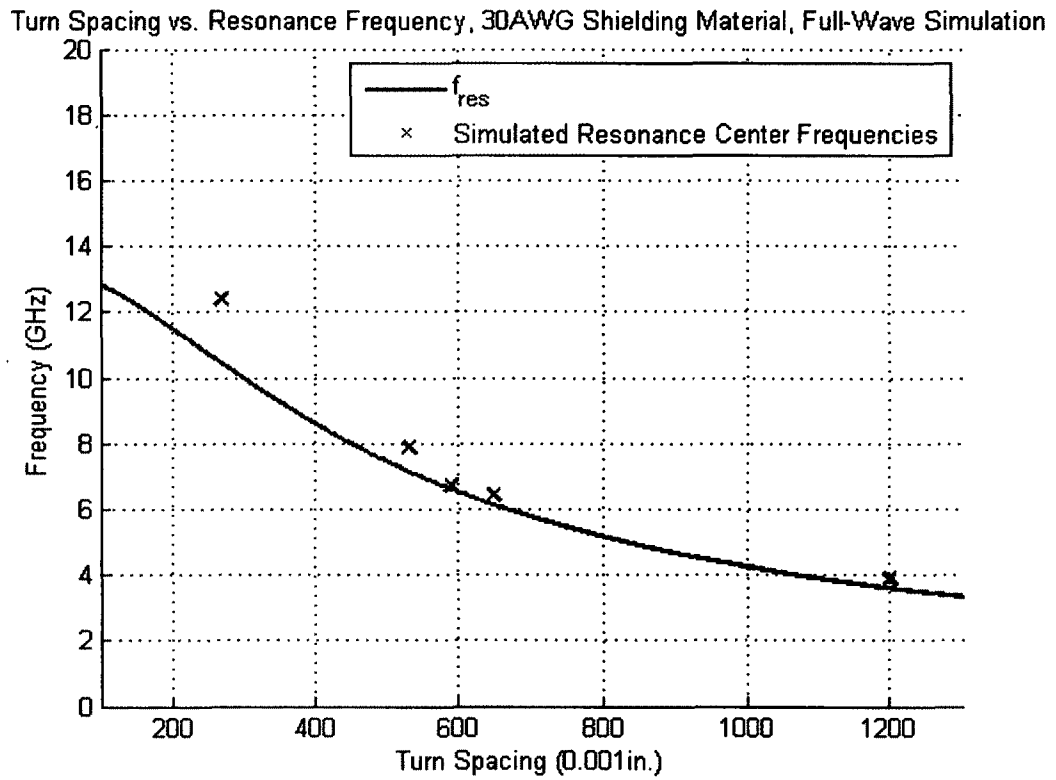


Figure 52: Full-Wave Simulated Resonance vs. Predicted Resonance, 30 AWG Spiral Shields

Figure 53 illustrates center frequencies obtained from circuit analyses against predicted resonance center frequencies.

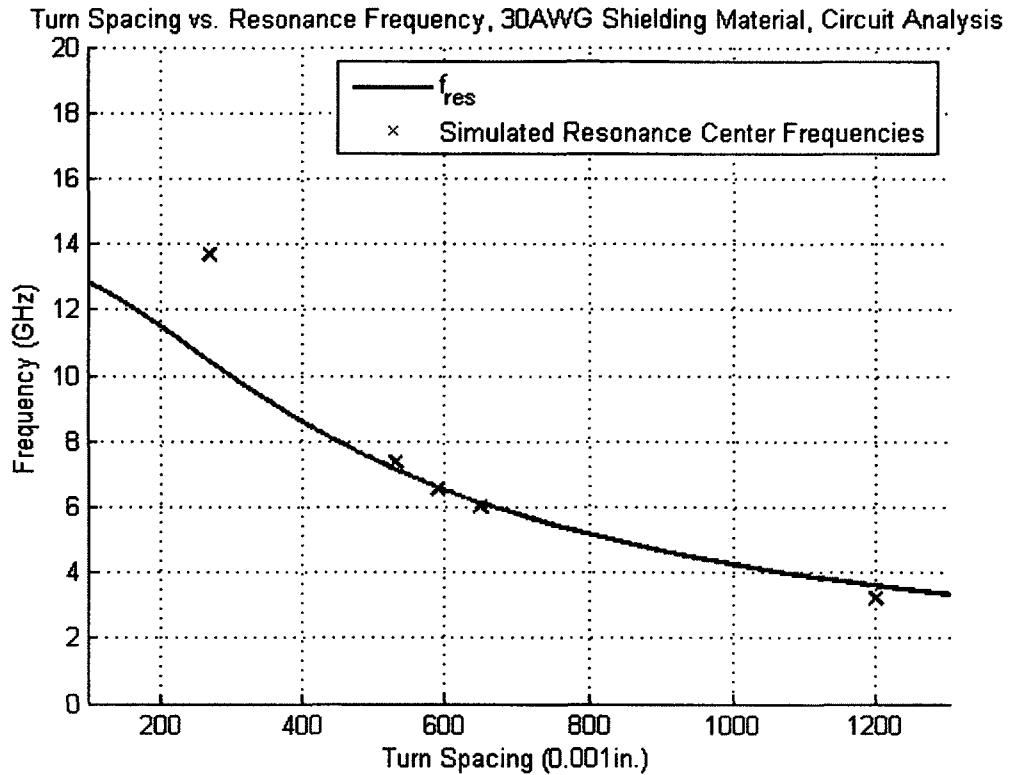


Figure 53: AC Analysis Resonance vs. Predicted Resonance, 30 AWG Spiral Shields

From Chapters 3 and 4, trends are illustrated by experiments performed in this study. Transmission line length does not impact the resonant frequency of the spirally wrapped twinaxial transmission line. However, as the turn spacing decreases, the center frequency of the resonant behavior in a differential transmission line increases. This is true regardless of wrap thickness and geometry as is illustrated in Figure 26. The most significant factors in approximating the resonant frequency in the DUT are the turn spacing dimension, the outside diameter of the dielectric material encasing the signal conductors, and the velocity of propagation of the transmission line. The range of impact

of each variable on the predicted resonance center frequency, f_{res} , is tabulated in Table 10. Three variations in turn spacing are examined. Turn spacing and diameter of the dielectric material are varied by 20% from the nominal value. Nominal values of phase velocity and dielectric diameter are $2.27 \cdot 10^8$ meters per second and 0.065 inches respectively. Nominal values for turn spacing are 0.270 inches, 0.590 inches, and 1.200 inches. Turn spacing variation has significant impact on center frequency throughout each range of nominal turn spacings. Conversely, dielectric diameter has more significant impact on center frequency as turn spacing decreases.

	Center Frequency Range, Turn Spacing = 0.270in.	Center Frequency Range, Turn Spacing = 0.590in.	Center Frequency Range, Turn Spacing = 1.200in.
Turn Spacing $\pm 20\%$	10.41 \pm 0.81GHz	6.63 \pm 1.01GHz	3.63 \pm 0.69GHz
Dielectric Diam. $\pm 20\%$	10.43 \pm 1.26GHz	6.59 \pm 0.32GHz	3.58 \pm 0.05GHz

Table 10: Magnitude of Center Frequency Variance Calculated From Equation 3

CHAPTER 6: Conclusions and Future Work

Chapter 6 reviews previous chapters and highlights key results from measurement, full-wave simulation, and circuit analysis. Considerations include scrutiny of the predictive equation discussed throughout this thesis, sources of calibration and measurement error, and possible sources of simulation error. This chapter suggests possible future simulation and experimental work to be done.

6.1 Measurements and Fixturing

The resonance frequency was observed to be independent of transmission line length in the measurements of commercially available twinaxial cables. The resonant frequency of these cables was in agreement with predicted values. Transmission data provided by the DUT showed that the resonant frequency depends on the turn spacing, which increases as the turn spacing decreases. The derived equation was able to predict the center of the resonance within 3.52% (mean) of the measured data for the aluminized polyester shield geometry. For 30 AWG shields, the predictive equation was within 3.11% (mean) of measured data. Percent deviations for both shield types are shown in Table 11 and Table 12.

Turn Spacing (Inches)	Measured Resonance Center Frequency (GHz)	f_{res} (GHz)	% deviation
1.200	3.76	3.44	4.73
0.850	4.84	4.69	1.22
0.649	6.48	5.87	5.71
0.590	6.78	6.32	2.73
0.530	7.14	6.84	0.13
0.400	8.56	8.22	0.35
0.270	10.11	9.97	2.98
0.200	11.06	11.00	3.74
0.160	13.30	11.56	10.01

Table 11: % Deviation Measured vs. Predicted Resonance Frequencies for Aluminized Polyester Shields

Turn Spacing (Inches)	Measured Resonance Center Frequency (GHz)	f_{res} (GHz)	% deviation
1.200	3.54	3.59	1.39
0.850	4.80	4.90	2.04
0.649	6.30	6.13	2.77
0.590	6.78	6.60	2.72
0.530	7.46	7.15	4.34
0.400	8.60	8.59	0.16
0.270	10.28	10.42	1.34
0.200	11.74	11.49	1.83
0.160	13.46	12.08	11.42

Table 12: % Deviation Measured vs. Predicted Resonance Frequencies for 30 AWG Shields

Error in the DUT measurements in this study come from three sources. The first originates from the manual technique used to construct the spiral shields. As turn spacings decreased there was an increase in difficulty to control the dimension of each individual turn as the shield is not fixed to the cable as it is being applied. However, the error in turn spacing was less when a foil was used as it is easier to wrap. The second source of error in measurement occurred in the fixturing used to measure the experimental DUT structures since the fixturing introduces impedance discontinuities and appreciable phase mismatches between the differential signal conductors. The third source of error in the s-parameter measurements comes from the calibration technique which does not de-embed the test signal connections. For s-parameter measurements collected on commercial twinaxial cables, error comes only from the fixturing and calibration technique.

6.2 Full-Wave Simulation

The general shapes of the resonances computed by the full-wave software tool are in fair agreement with the measurements for similar structures. Full-wave results for center frequency of the resonances were within 8.77% of the predictive equation on average. Percent deviation between f_{res} and simulated results are shown in Table 14.

Turn Spacing (Inches)	Simulated Resonance Center Frequency (GHz)	f_{res} (GHz)	% deviation
1.200	3.88	3.59	8.08
0.649	6.44	6.13	5.06
0.590	6.72	6.60	1.82
0.530	7.86	7.15	9.93
0.270	12.40	10.42	19.00

Table 13: % Deviation Simulated vs. Predicted Resonance Frequencies for Full-Wave Simulations

Sources of disagreement between full-wave results and the measured and predicted values are from error in material properties assumed in the full-wave model, uncompensated boundary conditions applied to the simulation space, and from the act of discretizing the structure.

6.3 Circuit Analysis

An approximate circuit model was created for a twinaxial structure wrapped with 30 AWG wire. Capacitance and inductance values were calculated by a quasi-static analysis of the 2D structure. The circuit model analysis results are in close agreement with the measurements and predicted values for the center frequency and were within 9.41% on average. Excluding the outlying data point (for a 0.270 inch turn spacing) reduces the mean deviation to 3.96%. Percent deviation between f_{res} and simulated results are shown in Table 14.

Turn Spacing (Inches)	First Resonance Center Frequency (GHz)	f_{res} (GHz)	% deviation
1.200	3.22	3.59	10.31
0.649	5.99	6.13	2.28
0.590	6.56	6.60	0.61
0.530	7.34	7.15	2.66
0.270	13.67	10.42	31.19

Table 14: % Deviation Simulated vs. Predicted Resonance Frequencies for Circuit Analyses

6.3 Conclusions

From the measurements and simulations, the resonance frequency was found to be dependent on the turn spacing and independent of transmission line length. The resonance frequency's wavelength corresponds to double the length of one turn of the applied spiral shield. The resonance frequency was independent of shield geometry. The predictive equation also depends on the transmission line's propagation constant. Verification of this finding was done with calibrated measurement on experimental structures, full-wave simulations, and quasi-static lumped element analyses. The fixture and DUT designed for this study were shown to be adequate for modeling spiral shield

behavior for a differential transmission line. Simulation methods performed for this study were promising in predicting the resonant behavior of the differential twinaxial structure.

Table 15 summarizes results of measurement and simulation compared to predicted center frequency for structures with 30 AWG applied as the shield.

Turn Spacing	Measured Resonant Frequency (GHz)	Resonant Frequency From Full-Wave Simulation Results (GHz)	Resonant Frequency From Circuit Analyses (GHz)	f_{res} (GHz)
1.200in.	3.54	3.88	3.22	3.59
0.649in.	6.30	6.44	5.99	6.13
0.590in.	6.78	6.72	6.56	6.60
0.530in.	7.46	7.86	7.34	7.15
0.270in.	10.28	12.40	13.67	10.42

Table 15: Measurement and Simulation Results Compared to the Predicted Resonance for 30 AWG shields

6.4 Future Work

Further work can be done in the measurement and simulation realms. Additional measurement fixture and baseline DUTs can be constructed of different lengths. Different signal conductors with larger diameter dielectric materials encasing them can be utilized in the DUT. Transmission measurements can be collected on these new structures. A ground drain wire can be included in the DUT to more closely approximate a commercial twinaxial cable.

Discretizing a spiral structure with smooth curves is difficult to perform accurately without utilizing considerable computational resources. Closer agreement between simulation and measurement of DUT structures might be possible with alteration

of the simulation model by including identical terminations. Full-wave simulation results may benefit from finer granularity in the discretization of the model.

Circuit-model analysis results may be improved and may show increased detail in transmission if the circuit model is broken into more π networks. Additional π network models will represent smaller percentages of the turn spacing of the transmission line, than those currently implemented. Lossy components might also be included in the model to more accurately model transmission characteristics. Many sections of the full π model may be cascaded to more accurately model transmission line behavior.

APPENDICES

APPENDIX A: Semi-Rigid Coaxial Cable Description

Chapter II presents the DUT structure that was constructed from two semi-rigid coaxial cables. These semi-rigid coaxial cables include two female Subminiature Version A (SMA) interconnects and a length of semi-rigid coaxial cable. Figure A 1 provides a mechanical drawing of the female SMA interconnect. Figure A 2 displays data from the semi-rigid coaxial line. These figures were provided by the cable manufacturer.

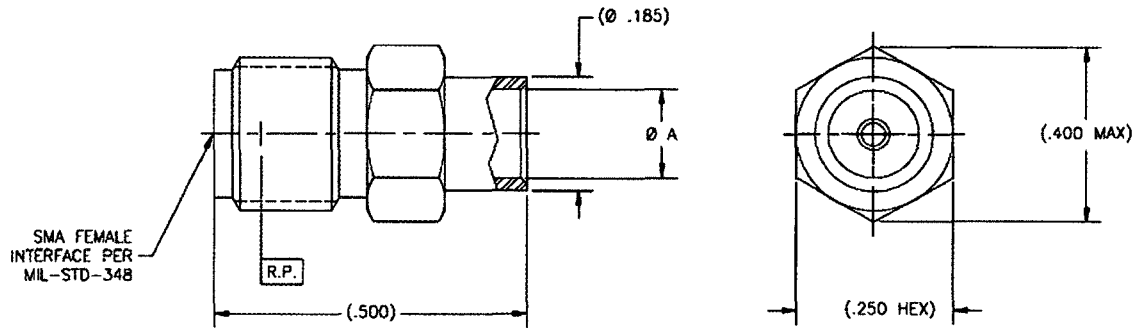


Figure A 1: Mechanical Drawing of Female SMA Interconnect

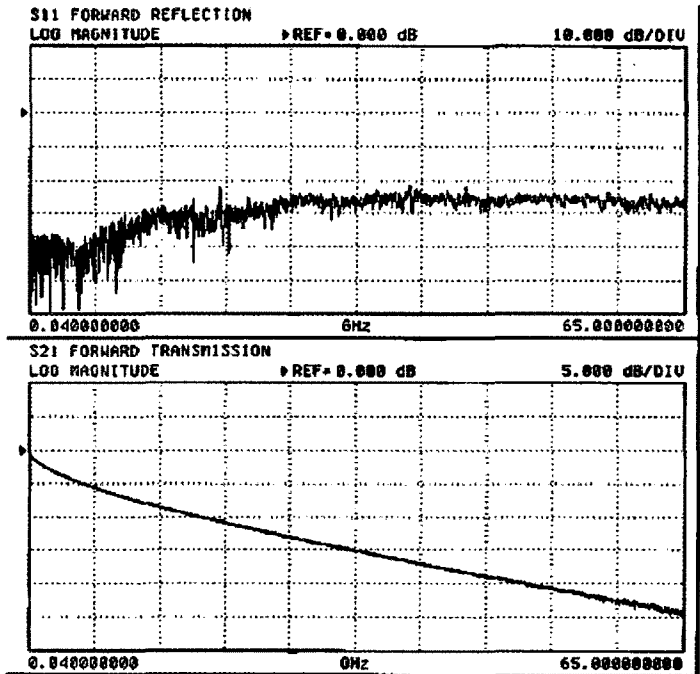
Anritsu

37397C

MODEL: UT085FORM 10FT DATE: 09/10/2007 18:08 Page 1
 DEVICE ID: LOT SFC400084 OPERATOR:

START: 0.04000000 GHz GATE START: - ERROR CORR: 12-TERM
 STOP: 65.00000000 GHz GATE STOP: - AVERAGING: 1 PT
 STEP: 0.04060000 GHz GATE: - IF BNDWDTH: 1 KHz
 WINDOW: -

PARAMETER:	-----CH1-----	-----CH3-----
NORMALIZATION:	-S11-	-S21-
REFERENCE PLANE:	OFF	OFF
SMOOTHING:	1.4908 cm	0.1034 mm
DELAY APERTURE:	0.0 PERCENT	0.0 PERCENT



SWEEP SETUP
 ▶START 0.040000000 GHz
 STOP 65.000000000 GHz
 SET CENTER/SPAN
 1601 DATA POINT(S)
 0.040600000 GHz
 STEPSIZE
 C.H. MODE OFF
 MARKER SWEEP
 DISCRETE FILL
 HOLD BUTTON
 FUNCTION
 TEST SIGNALS
 PRESS <ENTER>
 TO SELECT
 OR TURN ON/OFF

Figure A 2: Semi-rigid Coaxial Transmission Line Datasheet

APPENDIX B: Commercial Twin Axial Data Sheet

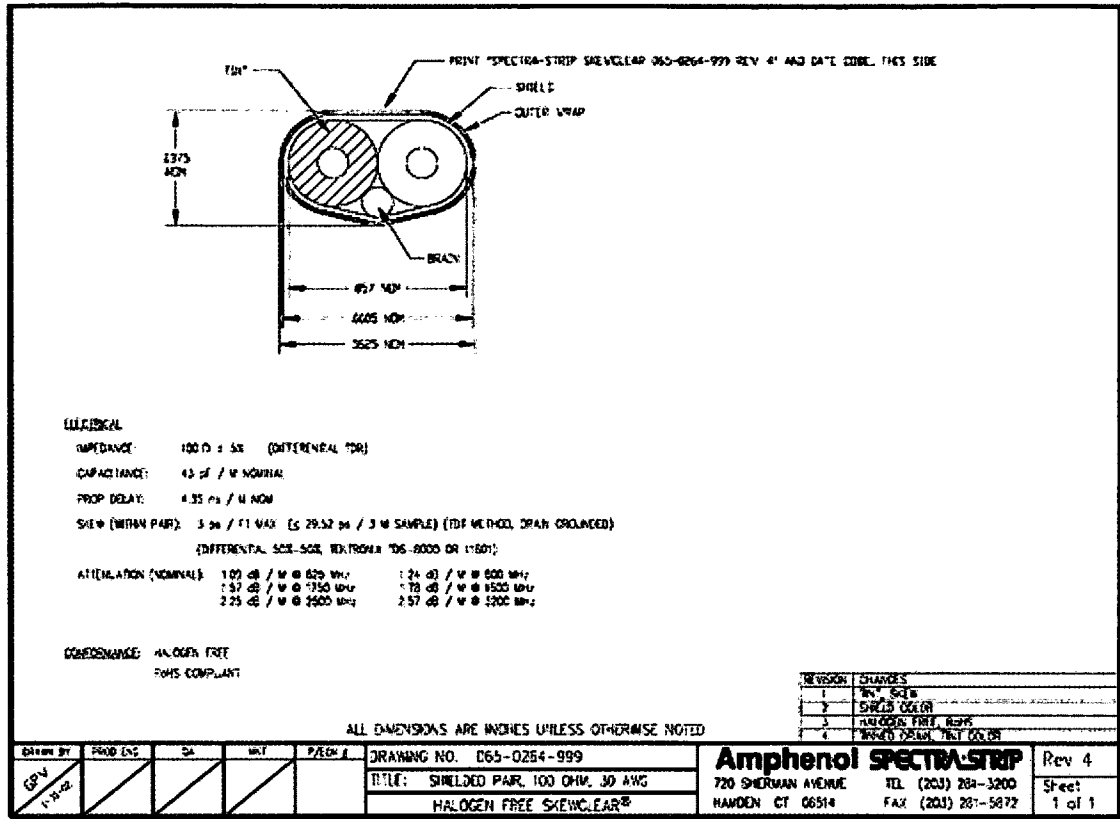


Figure B 1: Data Sheet for a Commercially Available Twinaxial Cable Assembly

APPENDIX C: Turn Length Calculation

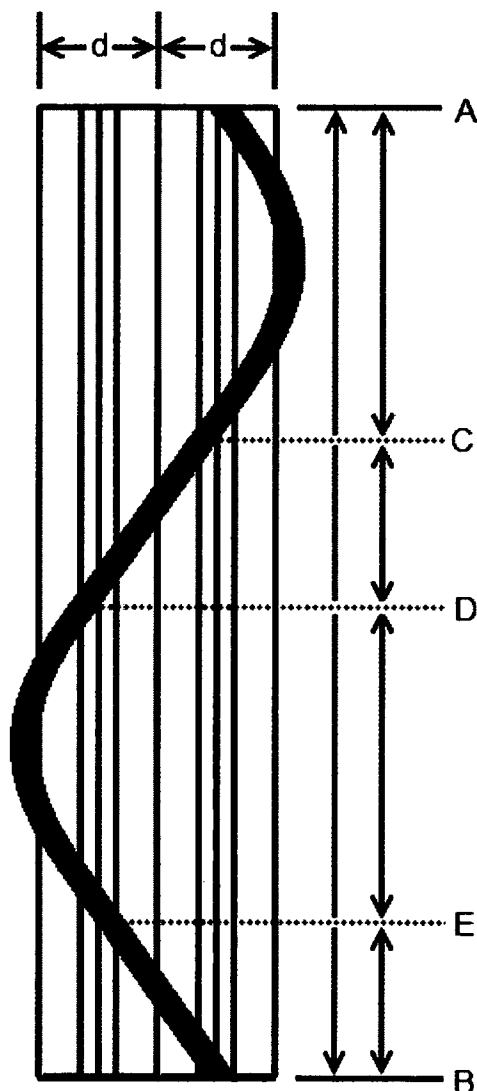


Figure C 1: Top view of one turn spacing

d = the diameter of dielectric.

Segment $AB = t$.

Segments **AC** and **DE** represent one turning phase of the spiral wrap. The length of this segment is calculated by Equation C1.

$$\sqrt{\left(\frac{\pi d}{2}\right)^2 + \left(t \frac{\pi d}{d(2+\pi)}\right)^2} \quad [C 1]$$

Segments **CD** and **EB** represent one straight phase of the spiral wrap. The length of this segment is calculated by Equation C2.

$$\sqrt{d^2 + \left(t \frac{d}{d(2+\pi)}\right)^2} \quad [C 2]$$

The turn length is the sum of two of each segment length quantity. The turn length is given in a simplified form in Equation C3.

$$l = \sqrt{t^2 + d^2(\pi + 2)^2} \quad [C 3]$$

APPENDIX D: Quasi-Static Simulation Tool Detail

Quasi-static simulation tools neglect the displacement current term in Maxwell's equations, and do not maintain the coupling between the electric and magnetic fields. Since the displacement current is neglected, quasi-static simulation tools are inaccurate when the structure is smaller than an eighth of one wavelength at a desired frequency.

Quasi-static electromagnetic field solvers calculate capacitance and admittance quantities from the solution of the electric field, and resistance and inductance values from the solution of the magnetic field. Quantities collected via the solution of the fields can then be placed into an equivalent circuit model in a SPICE based tool in order to compute the transfer function of the DUT.

The quasi-static simulation tool used in this study makes the following basic assumptions when solving for field quantities: 1) the structure being modeled only has quasi-TEM modes and has more than one conductor; 2) the transmission line is represented by a cross-section and is uniform; 3) only a small electric field component exists in the direction of wave propagation, all other fields lie in the transverse plane [Ans12]. The method used by this quasi-static tool is based on the finite element electromagnetic technique and the method of moments technique. The method used depends upon what quantity is calculated. Finite element method is used to solve direct current resistance, while the method of moments is used to compute inductance and capacitance quantities. With both techniques the two-dimensional modeled structures are segmented into polygonal elements upon which the electric and magnetic field quantities are calculated.

The Maxwellian Capacitance Matrix and a partial Inductance Matrix are computed by the quasi-static simulation tool. Maxwellian Capacitance Matrices quantify the relationship between conductors with respect to charge. For each conductor of a given simulation model, the charge and voltage relationship to each conductor is illustrated in this matrix format.

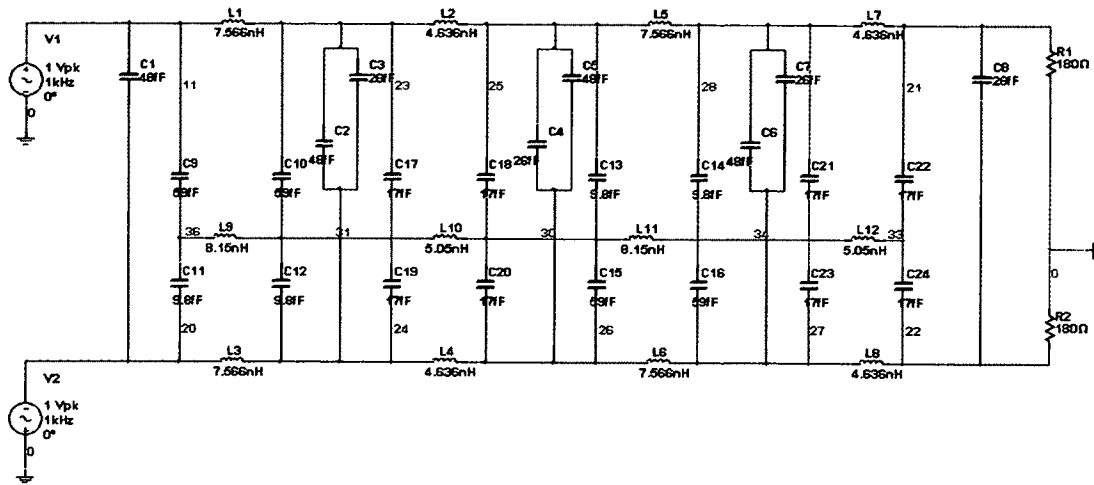


Figure E 3: Circuit Model, Twinaxial Structure, 30 AWG Spiral Shield, Turn Spacing of 0.590in.

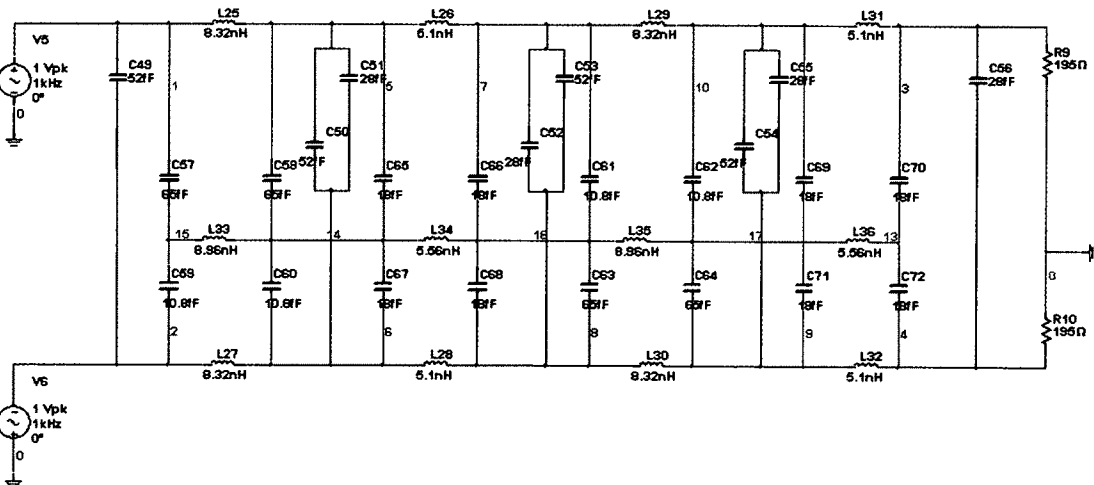


Figure E 4: Circuit Model, Twinaxial Structure, 30 AWG Spiral Shield, Turn Spacing of 0.530in.

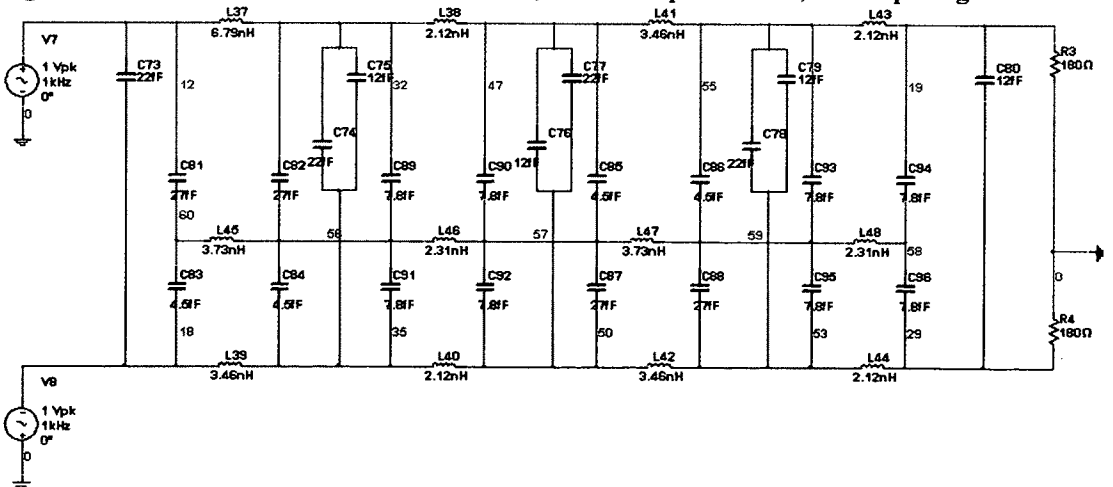


Figure E 5: Circuit Model, Twinaxial Structure, 30 AWG Spiral Shield, Turn Spacing of 0.270in.

LIST OF REFERENCES

- [Agi12] Agilent, Electronic Calibration (Ecal) Modules Reference Guide, Agilent, 2012.
- [And85] Anderson, Edwin M. Electric Transmission Line Fundamentals. Reston, Virginia: Reston Publishing Company, Inc., 1985.
- [Ans12] Ansys Corporation, Q3D Extractor Online Help, Ansys, 2012.
- [Ara08] D.N. Araujo, G. Pitner, M. Commens, B. Mutnury, J. Diepenbrock. "Full-Wave, TwinAx, Differential Cable Modeling." Electronic Components and Technology Conference, 58th, ECTC 2008 (May 2008), pp. 1684-1689.
- [Bog10] Bogatin, Eric. Signal and Power Integrity – Simplified. Second edition. Boston, Massachusetts: Prentice Hall, 2010.
- [Car07] Cartier, Marc, K. Sivaprasad. "A Measurement Based Comparison of Full-Wave and Quasi-static Methods for Baseband Modeling of Plated Through Hole structures to 20GHz." Electronic Components and Technology Conference, 57th, ECTC 2007 (May 2007), pp. 810-814.
- [Kur65] K. Kurokawa. "Power Waves and the Scattering Matrix." IEEE Transactions on Microwave Theory and Techniques, Vol. 13, No. 2 (March 1965), pp. 194-202.
- [Mat10] Matsumoto, Keisuke, Y. Toyota, K. Iokibe, R. Koga. "Development of Equivalent Circuit Model with Transmission Line Model for Designing Filters on Printed circuit Boards." Electromagnetic Compatibility (EMC), 2010 IEEE International Symposium (July 2010), pp 289-294.
- [Nab92] Nabors, Keith, S. Kim, J. White, "Fast Capacitance Extraction of General Three-Dimensional Structures" IEEE Transactions on Microwave Theory and Techniques, Vol. 40, NO. 7, July 1992.
- [Ram53] Ramo, Simon, and J. Whinnery. Fields and Waves in Modern Radio. Second edition. New York, NY: John Wiley & Sons, 1953.
- [Sch96] Schuhmann, R., M. Clemens, P. Thoma, and T. Weiland, "Frequency and Time Domain Computations of S-Parameters Using the Finite Integration Technique," Proc. of the 12th Annual Review of Progress in Applied Computational Electromagnetics (ACES Conference), Monterey, 1996, pp. 1295-1302.

- [Van03] Van Der Burgt, Martin. "Coaxial Cables and Applications." Belden Electronics Division, 2003.
- [Zha11] Zhang, Jianmin, H. Wang, J. Lim, K. Qiu, R. Brooks, and B. Chen. "Signal transition structure optimization for 16Gbps SFP cage and PCB interface," Electromagnetic Compatibility (EMC), 2011 IEEE International Symposium (August 2011), pp 785-790.